SYNTHESES, CHARACTERISATIONS AND ELECTROCHEMICAL STUDIES OF NICKEL(II) AND COBALT(II)-LIGAND ASSISTED COOPERATIVE COMPLEXES

JEEVITHRA DEWI A/P SUBRAMANIAM

FACULTY OF SCIENCE
UNIVERSITI MALAYA
KUALA LUMPUR

2020

SYNTHESES, CHARACTERISATIONS AND ELECTROCHEMICAL STUDIES OF NICKEL(II) AND COBALT(II)-LIGAND ASSISTED COOPERATIVE COMPLEXES

JEEVITHRA DEWI A/P SUBRAMANIAM

DISSERTATION SUBMITTED IN FULFILMENT OF THE REQUIREMENTS FOR THE DEGREE OF MASTER OF SCIENCE

DEPARTMENT OF CHEMISTRY
FACULTY OF SCIENCE
UNIVERSITI MALAYA
KUALA LUMPUR

2020

UNIVERSITI MALAYA

ORIGINAL LITERARY WORK DECLARATION

Name of Candidate: **JEEVITHRA DEWI A/P SUBRAMANIAM**

Matric No: **SGR 160049**

Name of Degree: **MASTER OF SCIENCE (EXCEPT MATHEMATICS & SCIENCE PHILOSOPHY)**

Title of Project Paper/Research Report/Dissertation/Thesis ("this Work"):

SYNTHESES, CHARACTERISATIONS AND ELECTROCHEMICAL STUDIES OF NICKEL(II) AND COBALT(II)-LIGAND ASSISTED COOPERATIVE COMPLEXES

Field of Study: **INORGANIC CHEMISTRY**

I do solemnly and sincerely declare that:

(1) I am the sole author/writer of this Work;
(2) This Work is original;
(3) Any use of any work in which copyright exists was done by way of fair dealing and for permitted purposes and any excerpt or extract from, or reference to or reproduction of any copyright work has been disclosed expressly and sufficiently and the title of the Work and its authorship have been acknowledged in this Work;
(4) I do not have any actual knowledge nor do I ought reasonably to know that the making of this work constitutes an infringement of any copyright work;
(5) I hereby assign all and every rights in the copyright to this Work to the University of Malaya ("UM"), who henceforth shall be owner of the copyright in this Work and that any reproduction or use in any form or by any means whatsoever is prohibited without the written consent of UM having been first had and obtained;
(6) I am fully aware that if in the course of making this Work I have infringed any copyright whether intentionally or otherwise, I may be subject to legal action or any other action as may be determined by UM.

Candidate's Signature Date: 12 June 2020

Subscribed and solemnly declared before,

Witness's Date: 18 June 2020

Signature Name:

Designation:

SYNTHESES, CHARACTERISATIONS AND ELECTROCHEMICAL STUDIES OF NICKEL(II) AND COBALT(II)-LIGAND ASSISTED COOPERATIVE COMPLEXES

ABSTRACT

A newly designed tetradentate ligand **L1** (**L1** = 3,6-bis(pyrazol-1-yl)-pyridazine) which offers multinucleation sites on its moiety structure has been prepared. The reaction of **L1** with different molar ratio of nickel and cobalt salts lead to the formation of di- and tetranuclear complexes $[Ni^{II}_2(\mathbf{L1})_2(CH_3CN)_4](PF_6)_4$ (**1**), $[Ni^{II}_4(\mathbf{L1})_4(\mu\text{-}OH)_4](ClO_4)_4$ (**2**) and $[Co^{II/III}(\mathbf{L1})_4(\mu\text{-}CH_3O)_2(\mu\text{-}O)_2](PF_6)_3(NO_3)$ (**3**), which served as the attempt to design of catalysts based on cheap and earth-abundant metals for carbon dioxide reduction. The presence of 1,8-diazabicyclo[5.4.0]undec-7-ene (DBU) as the base controls the nuclearity of the complex formation. In the absence of DBU, complex **1** was formed in dinuclear fashion whereas complex **2** and **3** formed tetranuclear fashion in the presence of DBU. The three complexes were structurally characterised by elemental analysis, nuclear magnetic resonance spectroscopy (NMR), Fourier transform infrared analysis (FT-IR), X-ray diffraction analysis, and voltammetry studies. Crystal structures revealed all complexes are centrosymmetric and adopted slightly distorted octahedral geometry. Complex **1** crystallises in monoclinic *C*2/*c* space group as the Ni(II) centre is octahedrally bound to **L1** in a *trans*-isomer arrangement. Complex **2** crystallises in tetragonal $I4_1/amd$ space group with four **L1** and four hydroxy bridging ligands linked to Ni(II) centre in *cis*-isomer arrangement. Complex **3** crystallises in orthorhombic C*mm* space group with four **L1**, two methoxy bridging ligand and two oxo bridging ligands linked to Co(II/III) centre in *cis*-isomer arrangement. FTIR confirmed the **L1** and bridging ligands were bound to the metal centre by exhibiting the shift at $\nu_{N=N}$, $\nu_{C=N}$, and $\nu_{C=C}$ stretching frequency of the free ligand. Cyclic voltammograms of **L1** and all complexes were measured under Ar and

CO_2. **L1** showed one reversible peak at -2.15 V vs. Ag/Ag^+ under Ar but the peak became irreversible under CO_2. Whereas the quasi-reversible peaks of complex **1** and **2** which appeared at -2.12 V and -2.16 V vs. Ag/Ag^+ respectively under Ar became irreversible and the current enhancement has occurred at that reduction under CO_2. Unlike complex **1** and **2**, even though complex **3** displayed a quasi-reversible peak at -2.19 V vs. Ag/Ag^+ under N_2 but neither irreversibility peak nor current enhancement was spotted at that potential under CO_2. In a sum, **L1** and the three complexes demonstrated redox behaviour under inert atmosphere and responded to CO_2 environment.

Keywords: Tetranuclear complexes, dinuclear complexes, tetradentate N6-ligand, carbon dioxide reduction

SINTESIS, PENCIRIAN DAN KAJIAN ELEKTROKIMIA BAGI KOMPLEKS NIKEL(II) DAN KOBALT(II) -DENGAN BANTUAN LIGAN

ABSTRAK

Ligan tetradentat baru **L1** (**L1** = 3,6-bis(pirazol-1-il)-piridazina) yang telah direka bentuk menawarkan tapak multinuklear pada struktur. Tindak balas **L1** dengan garam nikel dan kobalt dalam nisbah molar yang berlainan memainkan peranan untuk membentuk formasi kompleks dwi- dan tetranukleus $[Ni^{II}_2(\mathbf{L1})_2(CH_3CN)_4](PF_6)_4$ (**1**), $[Ni^{II}_4(\mathbf{L1})_4(\mu\text{-}OH)_4](ClO_4)_4$ (**2**) dan $[Co^{II/III}(\mathbf{L1})_4(\mu\text{-}CH_3O)_2(\mu\text{-}O)_2](PF_6)_3(NO_3)$ (**3**), dimana percubaan untuk menggunakan logam-logam bumi yang berlebihan and murah sebagai pemangkin penurunan karbon dioksida. Kehadiran bes 1,8-diazabisiklo[5.4.0]undek-7-ena (DBU) mengawal pengnukleasan formasi kompleks. Ketakhadiran bes menyebabkan pembentukan formasi komplex dwinukleus **1** manakala komplex **2** dan **3** membentuk formasi tetranukleus dengan kehadiran bes. Ketiga-tiga kompleks telah dicirikan secara struktur dengan analisis unsur, spekroskopi resonans magnet nucleus (NMR), spektroskopi transformasian Fourier inframerah (FT-IR), analisis pembelauan sinar-X dan kajian voltammetri. Kesemua komplex menunjukkan struktur hablur sentrosimetri dan menerima geometri herotan octahedron. Komplex **1** menghablur dalam kumpulan ruang monoclin *C*2/*c* dimana pusat Ni(II) terikat secara oktahedron dengan **L1** dalam penyusunan isomer-*trans*. Kompleks **2** pula menghablur dalam kumpulan ruang tetragon $I4_1/amd$ bersama empat **L1** dan empat hidroksi ligan titian terpaut dengan pusat Ni(II) dalam penyusunan isomer-*cis*. Komplex **3** menghablur dalam kumpulan ruang ortorombus C*mm* bersama empat **L1**, dua metoksi ligan titian dan dua okso ligan titian terpaut dengan pusat Co(II/III) dalam penyusunan isomer-*cis*. FTIR telah menyahkan **L1** dan ligan titian yang terikat dengan kompleks menunjukkan anjakkan pada frekuensi peregangan $\nu_{N=N}$, $\nu_{C=N}$ dan $\nu_{C=C}$. Voltammogram berkitar **L1** dan kompleks telah diukur dalam Ar dan CO_2. **L1** menunjukkan puncak berbalik pada -2.15 V *vs*. Ag/Ag^+ dalam Ar

manakala puncak tersebut tak berbalik dalam CO_2. Sementara puncak kuasi-berbalik kompleks **1** dan **2** pada keupayaan -2.12 V and -2.16 V *vs*. Ag/Ag^+ masing-masing dalam Ar telah menunjukkan puncak tak berbalik dan peningkatan arus dalam CO_2. Walaupun kompleks **3** menunjukkan puncak kuasi-berbalik pada -2.19 V *vs*. Ag/Ag^+ dalam N_2, puncak tak berbalik dan peningkatan arus tidak berlaku pada keupayaan tersebut dalam CO_2. Secara ringkas, **L1** and ketiga-tiga kompleks telah menunjukkan perlakuan redoks dalam atmosfera lengai dan memberikan respons terhadap CO_2.

Kata kunci: Kompleks tetranukleus, kompleks dwinukleus, N6-ligan tetrdentat, penurunan karbon dioksida

ACKNOWLEDGEMENTS

First and foremost, all praises to The Almighty God for His Mercy who has given me the strength, patience, and blessings to complete this work.

I would like to extend my deepest gratitude to my supervisor, Dr. Woi Pei Meng and co-supervisor, Associated Professor Shigeyuki Masaoka as well as Assistant Professor Mio Kondo for their invaluable guidance, suggestions, tolerance, and encouragement throughout my journey.

Not to forget, a warm thank you to D220 and D316 laboratory colleagues for their help and advice. Special gratitude to the Masaoka group laboratory working partners for their knowledge and lab skill guidance and emotional support throughout my 7 months attachment in Institute for Molecular Science, SOKENDAI, Japan.

Finally, I owe my deepest appreciation to my family and friends from UM for their love, concern, and support. None of this would have been possible without their love and support.

TABLE OF CONTENTS

LIST OF FIGURES

LIST OF TABLES

LIST OF SYMBOLS AND ABBREVIATIONS

^{1}H-NMR	:	Proton nuclear magnetic resonance
^{13}C-NMR	:	Carbon-13 nuclear magnetic resonance
Ar	:	Argon
CHN	:	Carbon, hydrogen, nitrogen elemental analyser
CO_2	:	Carbon dioxide
CV	:	Cyclic voltammetry
DBU	:	1,8-diazobicyclo[5.4.0]undec-7-ene
DMF	:	N,N-dimethylformamide
FE	:	Faradaic efficiency
FTIR	:	Fourier-transform infrared spectroscopy
GC	:	Glassy carbon
GC-MS	:	Gas chromatography mass spectrometer
HPLC	:	High performance liquid chromatography
H_2O	:	Water
CH_3CN	:	Acetonitrile
N_2	:	Nitrogen
SCXRD	:	Single crystal x-ray diffractometer
TFE	:	2,2,2-trifluoroethanol
TFEH	:	2,2,2-trifluoroethylhydrazine
TOF	:	Turnover frequency
TON	:	Turnover number
UV-vis	:	Ultraviolet-visible spectrophotometry

LIST OF APPENDICES

CHAPTER 1: INTRODUCTION

1.1 Background

Fossil fuel sources are holding the greatest fraction in energy supply to the world's necessities such as residential and commercial, transportation, and industrial usage (Dresselhaus, & Thomas, 2001). However, the rising energy demand will surpass the limited amounts of fossil resources in the future. It should be noted that fossil fuels have been used as precursors to manufacture various chemical products such as polymers, synthetic waxes. Chemical resources will be affected effectively with fossil fuel deficiency. Besides, the elevation of atmospheric CO_2 concentration is another serious issue arising from the mass consumption of fossil fuels (Li *et al.*, 2018). Over the years, fossil resource usage leads to the greenhouse gas effect gradually threatens human survival (Boot Handford *et al.*, 2014).

Further increases are predicted to produce large and uncontrollable impacts on the world climate. These projected impacts extend beyond climate to ocean acidification, because the ocean is a major sink for atmospheric CO_2 (Rosas Hernandez *et al.*, 2017). Granting a future energy supply that is secure and CO_2-neutral will require switching to non-fossil energy sources such as wind, solar, nuclear, and geothermal energy (Appel *et al.*, 2013)

Along this line to mitigate atmospheric CO_2, utilising CO_2 as a carbon energy source via carbon capture utilisation (CCU) technologies is one of the primary focuses of many countries (Do *et al.*, 2018; Simmons *et al.*, 2011). Electrocatalytic CO_2 reduction (Aresta, & Dibenedetto, 2007; Vidal Vázquez *et al.*, 2018) being part of the CCU technologies which prominently advancing in molecular level research for catalytic conversion of CO_2 into value-added chemical fuels and organic materials (Sampson *et al.*, 2014). Therefore, transforming CO_2 into a source of fuel or precursor for chemical products through

electrochemically offer an attractive way to decrease atmospheric concentrations. The challenges presented here are great, but the potential rewards are enormous.

The highly unfavourable reduction of thermodynamically stable CO_2 molecule (Schwarz, & Dodson, 1989) requires proton assisted multi-electron transfer reaction to lower the potential substantially and to produce thermodynamically more stable products (Benson *et al.*, 2009). This can be explained with carbon localised lowest unoccupied molecular orbital (LUMO) of CO_2 that is susceptible to attack by nucleophiles and resulted in reduction (Leitner, 1996). Converting CO_2 to a useful state by activation/reduction is a scientifically challenging problem, requiring appropriate catalysts and energy input.

Looking at our Mother Nature's biological system Ni-4Fe-5S cluster in CODHs enzyme (Dobbek *et al.*, 2001), utilises multinuclear clusters as the active centres to reduce CO_2 to CO that substantially used to yield energy. Governing a multinuclear core active centre for CO_2 reduction is a primitive idea from Nature's gift. As for now, the scientific world extensively studied the multinuclear clusters for water oxidation/reduction systems for greener fuel from oxygen and hydrogen gas respectively (Okamura *et al.*, 2016; Zhang, & Guan, 2019). The highlights of adopting a multinuclear core are imperative in multi-electron transfer (MET) for flexible redox process, reduction of overpotential of an electrocatalytic system (Okamura *et al.*, 2016; Praneeth *et al.*, 2019).

This research project is conducted to synthesis redox-active ligand and develop a multinuclear cluster system with cobalt and nickel metal. Electrochemical behaviour of the clusters analysed to evaluate the function of a multinuclear system as MET in CO_2 reduction.

1.2 Problem statement

The conversion of CO_2 into fuels employing solar energy remains a challenge for chemists. It would open the way to an economy based on renewable energy, and it would potentially give access to energy to everyone on earth. One may directly use light to perform the reactions or to preliminarily convert the light into electricity in photovoltaic cells and then use the electrons to reduce the carbon dioxide. Direct hydrogenation of CO_2 is another approach. Catalytic strategies are required to achieve the transformations due to the inertness of the substrate, but developing selective, efficient, and stable catalysts currently remains a highly challenging task (Takeda *et al.*, 2016).

1.3 Objectives of the study

This research project has the following aim and objectives:

I. To design a new multidentate redox ligand containing 3,6-bis(pyrazol-1-yl) pyridazine for the synthesis of multinuclear cobalt and nickel clusters.

II. To define and characterise synthesised ligand, cobalt, and nickel clusters with physicochemical and spectroscopy techniques such as single-crystal X-ray diffraction, elemental analysis, ^{1}H-NMR, ^{13}C-NMR, FTIR, UV-Vis Spectroscopy.

III. To analyse the electrochemical activity of the ligand, cobalt and nickel clusters under inert and CO_2 atmosphere using cyclic voltammetry and bulk electrolysis.

1.4 Thesis outline

This thesis is divided into 5 chapters consists of:

Chapter 1: Introduction

This chapter describes the overview of this research work, challenges in CO_2 reductions, problem statements as well as the objectives of this study.

Chapter 2: Literature review

In this chapter, relevant literature regarding CO_2 reduction utilising metal complexes as catalysts are discussed. The discussion started with the chemical and physical background of CO_2 reduction follows by electrocatalytic CO_2 reduction systems. Recent developments of multinuclear transition metal clusters as CO_2 reduction catalyst is discussed. The challenges facing this research field are reviewed as well.

Chapter 3: Materials and research methodology

The research methodology involved synthesis of redox ligand and multinuclear metal clusters. The synthesised ligand and clusters are characterised using FTIR, UV-Vis spectroscopy, single crystal XRD, CHN Elemental analysis, ^{1}H-NMR, and ^{13}C-NMR. The application run for CO_2 reduction was conducted through CV analysis and controlled-potential electrolysis. The gaseous and liquid products released are detected with GC-MS and HPLC, respectively.

Chapter 4: Results and discussion

This chapter describes the single crystal XRD data of the novel metal clusters designed. A detailed discussion of the nickel complex and cobalt complex

characterisation and activities towards CO_2 reduction under various manipulative variables are conducted as well.

Chapter 5: Conclusion and future works

The last chapter tabulates the summary of the main conclusion of this research and presents an outlook for future work.

CHAPTER 2: LITERATURE REVIEW

2.1 Transition metal complexes

Transition-metal complexes are at the cutting edge of potential catalyst research. These catalysts can have multiple and accessible redox states that have been proved to promote multi-electron transfer reactivity. Moreover, the formal reduction potentials can be systematically tuned through ligand modification to better match the potential required for CO_2 reduction (Morris *et al.*, 2009).

Transition-metal complex catalysts of CO_2 electrochemical reduction based on earth-abundant metals have been intensively reviewed (Savéant, 2008; Takeda *et al.*, 2016), with the description of the main classes of ligands (polypyridyl, phosphine, cyclam, and aza-macrocyclic ligands, porphyrins, phtalocyanines, and related macrocycles) and metals (Ni, Co, Mn, Fe), leading to efficient homogeneous electrochemical CO_2 reduction.

The first published crystal structure of CO_2 bound to a transition metal complex in 1975 was reported by Aresta and Nobile. Figure 2.1 illustrates the coordination geometry of η^2-bidentate binding mode involving the carbon atom and one oxygen atom, with significant bending in the CO_2 structure (Aresta *et al.*, 1975). This finding had proven the beneficial of transition-metal elements as electrocatalysts to facilitate the CO_2 reduction.

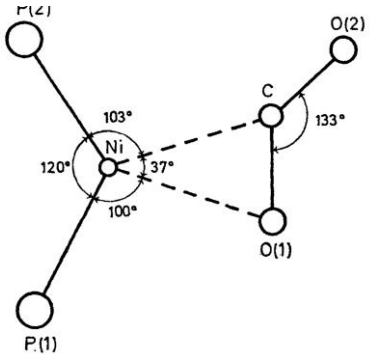

Figure 2.1: Mode of bonding of CO_2 in $[Ni(CO_2)(PCy_3)_2]$,0.75-toluene (Aresta *et al.*, 1975)

2.1.1 Cobalt complexes

Several investigations on cobalt complexes as a homogeneous catalyst for CO_2 reduction have been reported (Arana *et al.*, 1992; Chen *et al.*, 2015; Tinnemans *et al.*, 1984). The use of tetraazamacrocycle (Figure 2.2) was first investigated by (Che *et al.*, 1988; Tinnemans *et al.*, 1984).

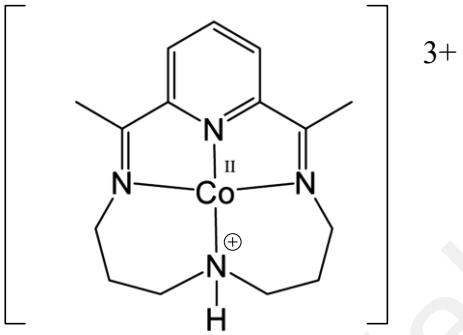

Figure 2.2: Cobalt tetraazamacrocycle (Che *et al.*, 1988; Tinnemans *et al.*, 1984)

Figure 2.3 illustrates the CV in acetonitrile at a carbon electrode produces CO in 20-30% faradaic yield at 940 mV overpotential, with no H_2 as a by-product. The active catalytic species was the Co^{I} ligand radical anion species (*i.e.*, the doubly reduced species issued from the Co^{II} neutral) (Takeda *et al.*, 2016).

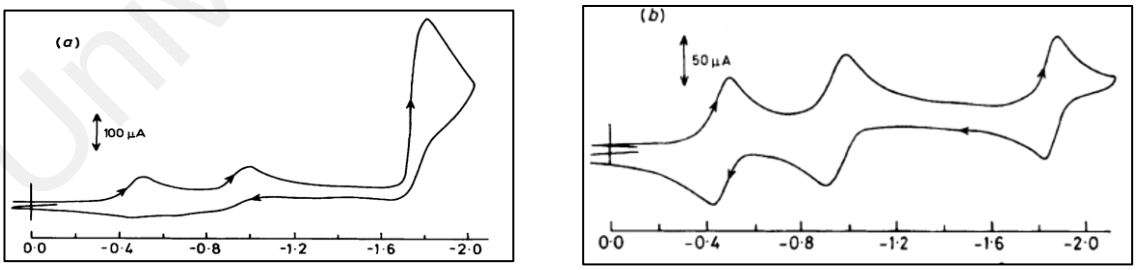

Figure 2.3: Cyclic voltammogram of *(ca.* 1 mmol) in 0.1 mol dm^{-3} $[NBu_4]BF_4$ in acetonitrile solution in *(a)* the presence and (b) the absence of CO_2. Working electrode, pyrolytic graphite; scan rate, 100 mVs^{-1}. Reprinted with the permission from (Che *et al.*, 1988). Copyright 1988 Dalton Transaction.

In recent studies, an efficient Co catalyst for the CO_2-to-CO conversion was discovered with four aminopyridine macrocycle as ligands, linked by pendant amine groups (Figure 2.4). Highly selective CO formation (98%) could be sustained for 2 hours in a DMF solution saturated with CO_2 and containing 1.2 M of trifluoroethanol as a weak acid to help the catalysis with 680 mV overpotential. In sum, 6.2 TON of CO was formed, and it was suggested that the pendant NH groups helps stabilise the Co^{I}-CO_2 adduct (Chapovetsky *et al.*, 2016; Takeda *et al.*, 2016). A comparative study of nickel complexes is summarised in Appendix A- 1.

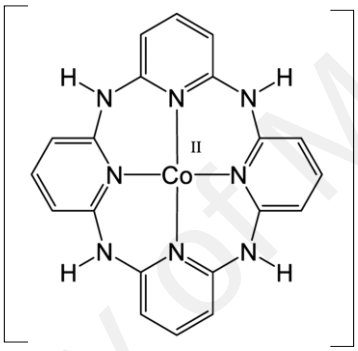

Figure 2.4: Cobalt aminopyridine macrocycle as ligands, linked by pendant amine groups (Chapovetsky *et al.*, 2016).

2.1.2 Nickel complexes

The d^8 electronic state in the valence orbital of nickel(II) favours a planar four coordinate geometry when it coordinates with organic ligands. Reported structures of tetraaza-macrocyclic planar ligands (Figure 2.5) possessing tetradentate atoms, resulting in stable nickel complexes (Beley *et al.*, 1986). Initially, Sauvage and co-workers discovered that nickel cyclam exhibits high catalytic activity and selectivity towards CO_2-to-CO conversion in the aqueous system at mercury working electrode (Beley *et al.*, 1986). Observation speculates that a strong chemical absorption between the surface of the mercury working electrode and the cyclam complex.

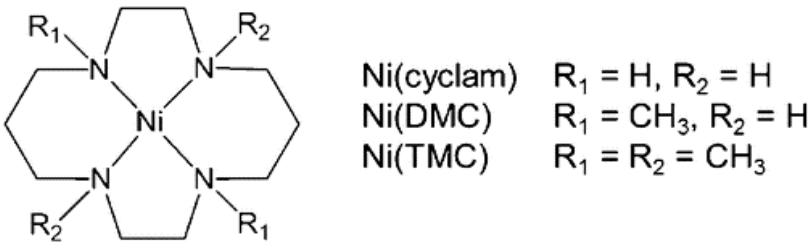

Figure 2.5: Structures of Ni(cyclam), Ni(DMC) (DMC = 1,8-Dimethyl-1,4,8,11-tetraazacyclotetradecane), and Ni(TMC) (TMC = 1,4,8,11-Tetramethyl-1,4,8,11-tetraazacyclotetradecane) (Beley *et al.*, 1986; Froehlich, & Kubiak, 2012).

Several research had been conducted to revealing the high catalytic performance and summarised that this performance may be correlated with the employed working electrodes and the conformations of the cyclam ligand (Figure 2.6) (Froehlich, & Kubiak, 2012; Wu *et al.*, 2017). A control experiment using a glassy carbon electrode instead of mercury working electrode was performed and found that CO_2 reduction by Ni(cyclam) was a homogeneous reaction. However, a lower efficiency was obtained with the glassy carbon electrode than with the mercury electrode. This may due to that the mercury

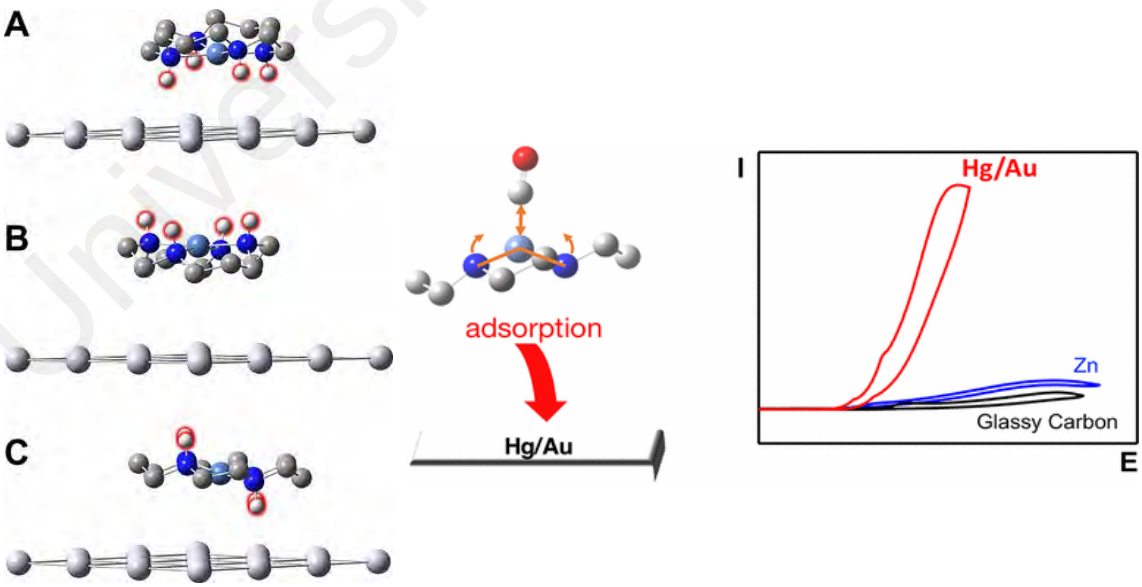

Figure 2.6: Correlating between employed working electrodes and the conformations of the cyclam ligand. Optimised geometries of (A) *trans*-I cap, (B) *trans*-I bowl, and (C) *trans*-III $[Ni(cyclam)]^+$ on an Hg surface (Wu *et al.*, 2017).

induced favourable electronic effects to facilitate CO_2 binding to Ni^I as in Figure 2.6 (Froehlich, & Kubiak, 2012; Wu *et al.*, 2017).

It is well known that cyclam complexes were reported extensively since the 1980s. Ligands such as macrocycle (Meshitsuka *et al.*, 1974), polypyridine (Lam *et al.*, 1995), and N-heterocyclic carbene (Thoi *et al.*, 2013) based nickel complexes were emerging in electrocatalytic CO_2 reduction as well (Figure 2.7). A comparative study of nickel complexes is summarised in Appendix A- 2.

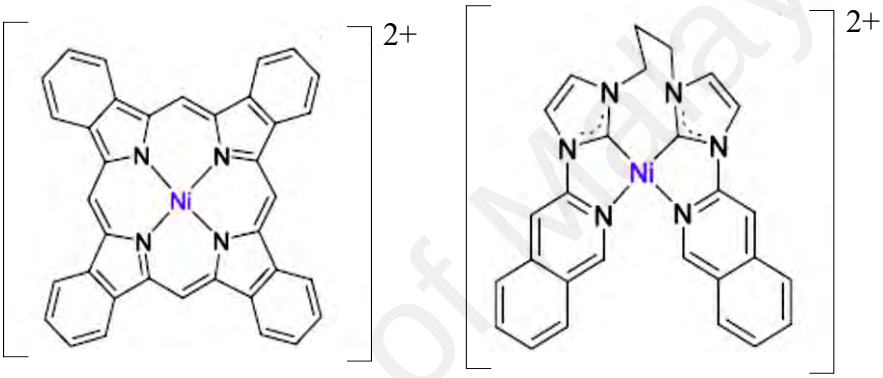

Figure 2.7: (Left) nickel phthalocyanine; (right) nickel N-heterocyclic carbene.

2.2 Redox-active ligand

Nature's use of redox-active moieties combined with 3d transition metal ions is a powerful strategy to promote multi-electron catalytic reactions. The ability of these moieties to store redox equivalents helps metalloenzymes in promoting multi-electron reactions. In a biomimetic spirit, chemists have recently developed approaches relying on redox-active moieties in the environment of metal centres to catalyse challenging transformations (Praneeth *et al.*, 2012).

Redox-active ligands with larger π-π conjugation often facilitate crucial multi-electron catalytic transformations. The dependency of nature on redox-active moieties to catalyse challenging reactions, either bound as ligands or in the second coordination sphere of a

metal cofactor. Nature utilises redox-active moieties to store and mediate electron-transfer to metal centres thereby communicating noble metals and 3d transitional metals such as Fe, Co onto base metals (Praneeth *et al.*, 2012; Rakowski Dubois, & Dubois, 2009).

The properties and behaviours of transition metal complexes rely on bridging ligand as it can hold one or more transition metals together. The bridging ligand can act as electronic communicators between the metal centres and depending on their structures, they can act as electronic insulators too. In addition, the nature and topology of the ligand allow the metals to cooperate for a specific reaction (García Antón *et al.*, 2012).

For example, Tanaka and the co-workers demonstrated the electrochemical water oxidation reaction using a ruthenium catalyst containing an *o*-quinone ligand as shown in Figure 2.8. Quinone adopts 3 different oxidation states: 1) quinone, 2) semiquinone, and 3) catecholate. The resulting dinuclear complex displays tremendous water oxidation activity with high turnover numbers (TON> 30 000). Comparing to other water-oxidation catalysts, which rely on high valent ruthenium oxo species, Tanaka's system shuttled between Ru^{II} and Ru^{III}, coupled with ligand-centred (i.e. semiquinone/ quinone) redox couples (Ghosh, & Baik, 2011; Wada *et al.*, 2000, 2001).

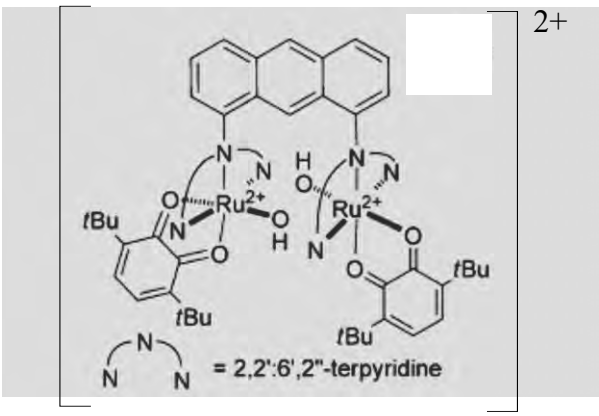

Figure 2.8: Tanaka's system bearing quinone moieties. Tanaka's system involves redox changes at the quinone moiety combined with a Ru^{II}/Ru^{III} couple.

Peng Kang and co-workers have developed an imino bipyridine cobalt(II) complex (Figure 2.9) for electrocatalytic reduction of CO_2 to formate in acetonitrile which possesses π-conjugation system. The single tridentate ligand in this study allowed more open sites, and large steric of the diisopropyl moieties can prevent dimerization of the active hydride intermediate which contributed to increase catalytic reactivity. The redox-active imino bipyridine ligand was effective in delocalising electron density from the Co centre to the ligand, thus making the Co centre less electron rich (Liu *et al.*, 2018). Thus, employing redox-active ligand with transition metals as the electrocatalysts for CO_2 reduction enhances the efficiency and selectivity besides reducing the overpotential.

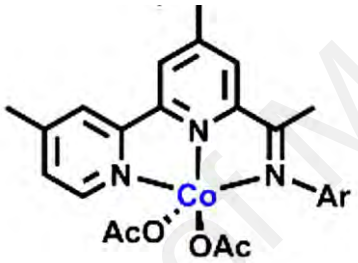

Figure 2.9: Imino bipyridine cobalt (II) complex.

2.3 [NiFe]-CO dehydrogenase enzyme as bio-inspired CO_2 reduction metal complex system

Nature's biological systems especially photosynthesis playing a vital part in balancing the carbon-neutral cycle. Enzymes have discovered to catalyse the reversible reduction of CO_2 to CO (CO dehydrogenases) or CO_2 to formate (formate dehydrogenases). The utilisation of 3d transition metals (Fe, Ni, Mo etc.) within the enzyme clusters is a significant design favoured by nature.

A popular enzyme known as CODH (CO dehydrogenases) has identified to catalyse CO_2 to CO. [NiFe]-CO dehydrogenase from Cluster C (Figure 2.10) with the active site consists of Ni and Fe centres bridged by an Fe_3S_4 cluster that rigidly positions these two

metal centres in close proximity. Scheme 2.1 describes the mechanism of [NiFe] CODHs in CO_2 reduction into CO (Appel *et al.*, 2013; Froehlich, & Kubiak, 2012; Jeoung, & Dobbek, 2007; Volbeda, & Fontecilla Camps, 2005).

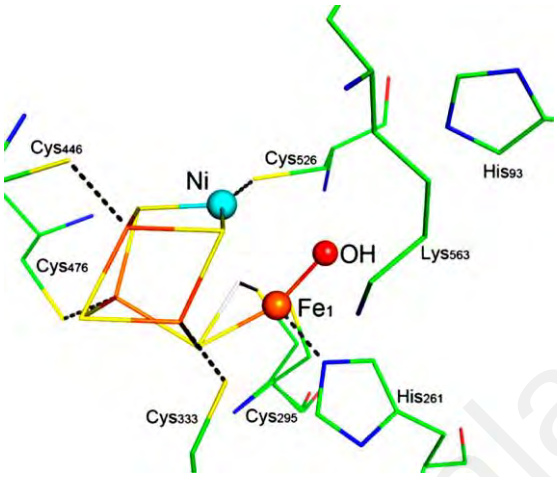

Figure 2.10: Ball-and-stick drawing of the active site of [NiFe] CO dehydrogenase (cluster C) (Jeoung, & Dobbek, 2007).

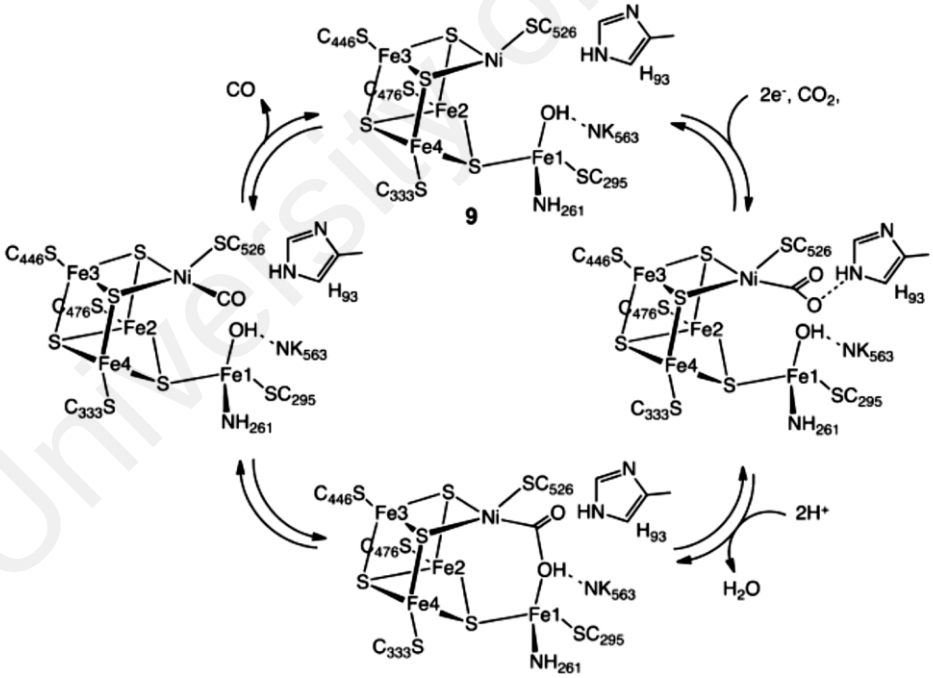

Scheme 2.1: Proposed mechanism for the reduction of CO_2 to CO by [NiFe] CODH (Jeoung, & Dobbek, 2007).

In conclusion, the extensive studies with cobalt and nickel complexes towards CO_2 reduction were primarily focused on mononuclear complexes. This means, fewer findings employed with multinuclear complexes for CO_2 reduction. Several findings by Schneider et.al and DeLaet et.al reported utilising trinickel phosphine and dinickel phosphine complexes for CO_2 reduction activity (DeLaet *et al.*, 1987; Schneider *et al.*, 2012a). However, the products formed were merely negligible (Appendix A- 2**Error! Reference source not found.**).

However, substantial research studies were conducted with multinuclear metal complexes employing redox-active ligand in the water oxidation system. Okamura and co-workers invented the most efficient catalyst to oxidise water with pentanuclear iron with redox-active ligand (**L**H:3,5-bis(2-pyridyl)pyrazole) (Figure 2.11) with Faradaic efficiency of 96% (Okamura *et al.*, 2016). The electrochemical analysis confirmed the redox flexibility of the system, characterised by six different oxidation states between $FeII_5$ and $FeIII_5$; the $FeIII_5$ state was active for oxidising water. They reported that creating a system with redox flexibility and contains adjacent small molecule activation sites could achieve efficient catalyst. Their strategy employing redox-active ligand that could hold multi-metal centres facilitate in achieving high efficiency. Relating to this

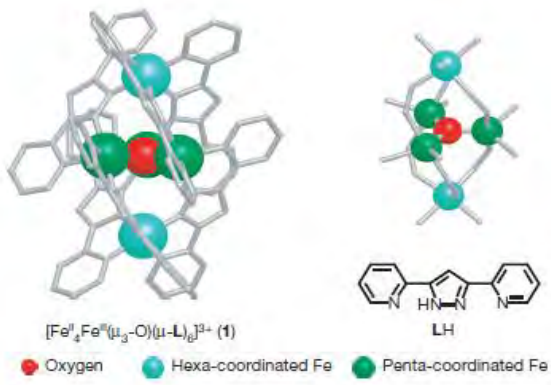

Figure 2.11: Pentanuclear iron catalyst for water oxidation (Okamura *et al.*, 2016).

concept, the niche of this research is to design a multinuclear metal complex with redox-active ligand to fill up gap exists in CO_2 reduction.

2.4 Conversion of CO_2 into value-added organics

In the midst of depleting carbon based natural resources, CO_2 is a promising and alternative carbon feedstock which is a renewable, cheap, safe, and non-flammable source to sustain the oil-based industries and economies (Sakakura *et al.*, 2007). The catalytic conversion of CO_2 to liquid fuels is a critical goal that would positively impact the global carbon balance by recycling CO_2 into usable fuels. CO_2 is reduced to give C1 or C2 compounds such as CO, formate, methanol, or oxalate as potential sustainable fuels or synthetic building blocks. The very common method is converting CO_2 into CO and H_2 precursors and utilise Fischer-Tröpsch technologies to synthesis value-added organic materials Figure 2.12.

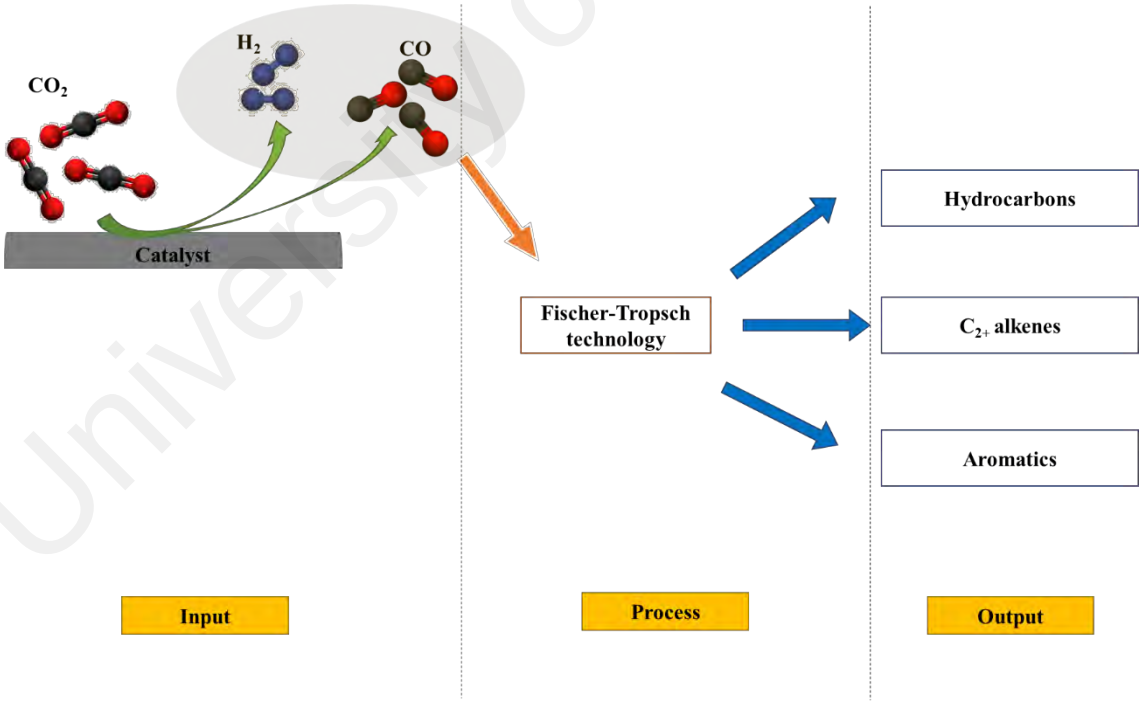

Figure 2.12: CO conversion into value-added organic products using CO_2 as the starting material.

Nevertheless, the direct activation of CO_2 for electrophilic or nucleophilic attack by a second substrate through prior complexation to a transition metal catalyst is a highly challenging task. The design and implementation of such direct activation strategies may help to define the shape of the future product portfolio based on this renewable carbon feedstock (Kleij, 2013; North, & Pasquale, 2009).

2.5 Activation of CO_2 by metal complex

Figure 2.13 shows several common coordination modes with transition metal compounds which involved CO_2 (Kleij, 2013; Vol'pin, & Kolomnikov, 1973):

a) ***η^1(C) coordination mode:*** via electron donation from metal to the carbon orbital with the formation of the metallo-acid derivative (preferred electron-rich metal ion)

b) ***η^1(O) coordination mode:*** via oxygen by donation of the oxygen lone p-electron pair to the vacant orbital of the metal (preferred electron-poor metal ion)

c) ***η^2 (C, O) coordination mode:*** via π-complex formation via C=O double bond. The "back-bonding" from filled metal *d*-orbitals to empty π*-orbitals from CO_2 plays an important role.

d) ***η^2 (O, O) coordination mode:*** binding type as "metal carboxylate"

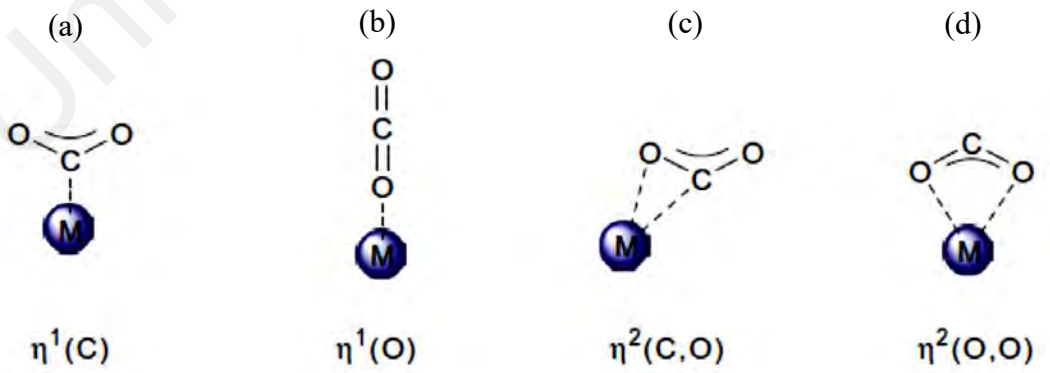

Figure 2.13: Mode of coordination with metal ion (Kleij, 2013; Paparo, & Okuda, 2017).

The coordination of CO_2 results in a net transfer of electron density from the metal to the LUMO of the ligand if the complexation takes place via the double bond or the central carbon atom. The LUMO of CO_2 is an antibonding orbital and therefore electron transfer should result in a weakened C-O interaction (Becker, 1992; Leitner, 1996). As the prime step to activate CO_2, it should accept an electron in its antibonding π orbitals that cause the molecule to bend (Refer to Figure 2.14).

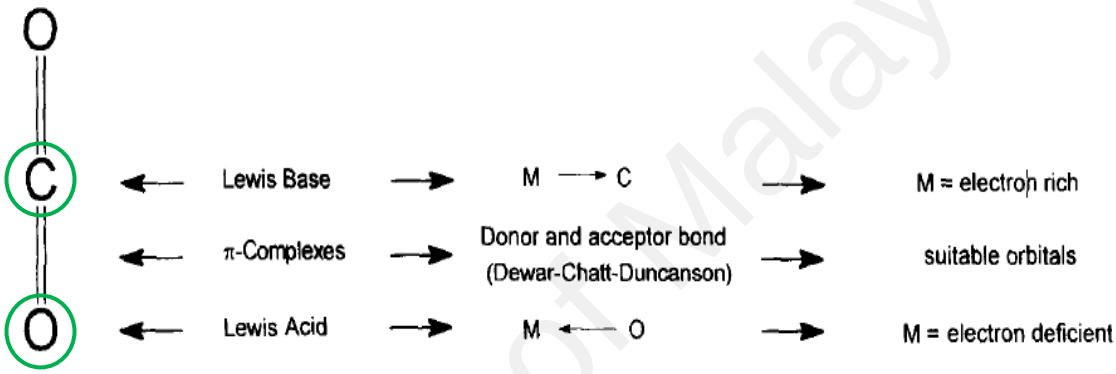

Figure 2.14: Reactive positions of the CO_2 molecule and the electronic properties of a transition metal centre required for complexation (Kleij, 2013; Leitner, 1996).

2.6 Electrochemical reduction of CO_2

It is now understood that CO_2 is thermodynamically and kinetically stable molecules that require a greater amount of energy to reduce into liquid fuels or fuel precursors such as synthetic gas (CO/H_2). From the in-depth discussion by Kleiji et al., Sakkura et al., and Benson et al. thermodynamic barrier and kinetic barrier are the two challenges in CO_2 reduction (Benson *et al.*, 2009; Kleij, 2013; Sakakura *et al.*, 2007). Thus, the utilisation of CO_2 via electrochemical reduction constitutes a promising approach toward the production of value-added chemicals or fuels using intermittent renewable energy sources (Francke *et al.*, 2018).

2.6.1 Thermodynamic barrier

CO_2 is highly unfavourable for one-electron reduction with higher E^o = -1.90 V *vs.* SCE, (E1) due to large reorganisational energy between the linear molecule and bent radical anion (Wang *et al.*, 2015). To lower the potential substantially, proton assisted multi-electron transfer reaction is required to produce thermodynamically more stable products. This is summarised in Table 2.1 (pH 7 in aqueous solution *vs.* SCE 25 ºC, 1 atm, and 1M for the other solutes) (Benson *et al.*, 2009).

Table 2.1: CO_2 reduction potentials at pH 7 and 1 atm in aqueous medium *vs.* SCE.

Reaction	E^o (V) *vs.* SCE	
$CO_2 + e^- \rightarrow CO_2^-$	E^o = -1.90 V	(E1)
$CO_2 + 2H^+ + 2e^- \rightarrow CO + H_2O$	E^o = -0.53 V	(E2)
$CO_2 + 2H^+ + 2e^- \rightarrow HCOOH$	E^o = -0.61 V	(E3)
$CO_2 + 4H^+ + 4e^- \rightarrow HCHO + H_2O$	E^o = -0.48 V	(E4)
$CO_2 + 6H^+ + 6e^- \rightarrow CH_3OH + H_2O$	E^o = -0.38 V	(E5)
$CO_2 + 8H^{+1} + 8e^- \rightarrow CH_4 + 2H_2O$	E^o = -0.24 V	(E6)

For the first reduction, there is a change in geometry from the linear CO_2 to a bent $CO_2^{-\bullet}$ where this structural change gave rise to a very slow self-exchange rate for the $CO_2/CO_2^{-\bullet}$ couple and contributed to a significant overpotential in the reduction of CO_2 (Keene, 1993). This is due to large reorganisation energy between the linear molecule and bent radical anion (Viswanathan, 2013). However, the formation of higher carbon products involved protons, reactions are more favourable at low pH. With the aid of proton assisted multi-electron transfer reaction, CO_2 reductions became more favourable in a thermodynamic aspect (Appel *et al.*, 2013; Benson *et al.*, 2009; Morris *et al.*, 2009; Yamase, & Sugeta, 1990).

The assembly of the nuclei and formation of chemical bonds to convert the relatively simple CO_2 molecules into more complex and energetic molecules is the significant setback in the CO_2 conversion. According to Kubiak and co-workers, there are two strategic ways to accomplish this. The easiest way is the conversion of CO_2 and H_2O into CO and H_2, utilise Fischer-Tröpsch technologies to produce value-added organics such as liquid fuels. The second strategy is known as "do it the hard way" through direct electrocatalytic conversion CO_2 into liquid fuels. The kinetic barrier is superior here. Any possibilities to overcome this challenge? One of the methods is to recognise a single catalyst that capable to perfect the sequence of conversion steps CO_2 to CO, then H_2CO, then to higher carbon molecules with low kinetic barriers. The difficulty of the transfer of multiple electrons to the site of the reduction is a limiting factor in the feasibility of such processes (Viswanathan, 2013).

Generally, formic acid and carbon monoxide which are belong to $2H^+/2e^-$ reduction products are produced in the reaction as compared to the rest, due to the difficulty of proton-coupled electron transfer process without any catalyst involved. While CO is a useful chemical and can be converted into liquid hydrocarbons via the Fischer– Tröpsch reaction with H_2. Formic acid has recently drawn attention as a carrier of H_2 because it is liquid at ambient temperatures (Johnson *et al.*, 2010; Rosas Hernandez *et al.*, 2017).

2.6.2 Electrocatalysis

Scheme 2.2 displays a general approach of an electrocatalytic system.

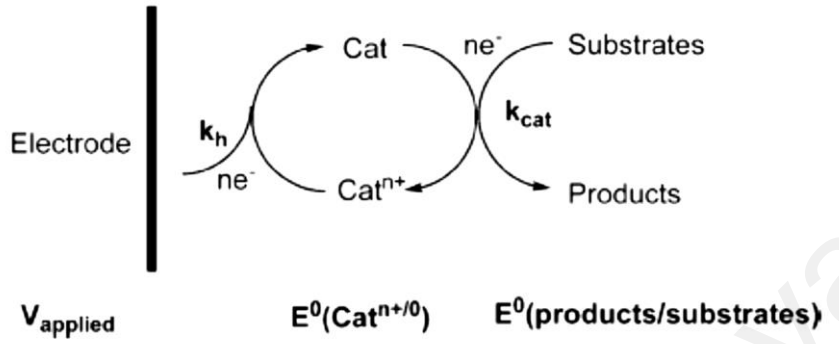

Scheme 2.2: A general approach of an electrocatalytic system (Benson *et al.*, 2009).

An electrocatalyst involved in an electron transfer reaction at the electrode and aid acceleration of a chemical reaction. For an efficient and optimal electrocatalyst, both the electron transfer and chemical kinetics required to be fast. Besides that, it should demonstrate an optimum thermodynamic match between the redox potential (E^0) for the electron transfer reaction and the chemical reaction that is being catalysed *i.e.* reduction of CO_2 to HCOOH (Benson *et al.*, 2009).

Generally, electrocatalysts were screened for their certain crucial features as listed below to determine the best overall catalysts (Benson *et al.*, 2009; Schneider *et al.*, 2012b).

1. Redox potentials
2. Current efficiencies
3. Electron transfer rate
4. Chemical kinetics

Electrocatalysts are electron transfer agents that ideally work near the thermodynamic potential of the reaction to be driven, E^0 (products/substrates). The direct electrochemical reduction of carbon dioxide on most electrode surfaces demands large overpotential which reduced the efficiency of conversion. One method to overcome the above issue is to utilise homogeneous redox catalysts in indirect electrolysis which lower kinetic barriers. This usually yields an increased and/or entirely different selectivity compared to direct electroreduction (Francke, & Little, 2014; Francke *et al.*, 2018; Rountree *et al.*, 2014).

The overpotential, η can be the differences between the applied electrode potential, $V_{applied}$, and E^0(products/substrates), at a given current density as refer to Equation 2.1.

$$\eta = V_{applied} - E^0(products/substrates) \qquad \text{(Equation 2.1)}$$

Both thermodynamic and kinetic considerations are important here. Clearly, to minimise overpotential, catalysts need to be developed to have formal potentials, E^0 ($Cat^{n+/0}$) which well-matched to E^0 (products/substrates), and appreciable rate constants, k_{cat}, for the chemical reduction of substrates to products at this potential. Moreover, the heterogeneous rate constant, k_h, for reduction of the electrocatalyst at the electrode must be high for $V_{applied}$ near E^0 ($Cat^{n+/0}$). Reaction rates for these processes can be estimated from the steady-state limiting current in cyclic voltammetry, or by rotating disk voltammetry studies of the heterogeneous electron transfer kinetics (Benson *et al.*, 2009; Francke *et al.*, 2018; Rountree *et al.*, 2014; Schneider *et al.*, 2012b).

2.6.3 Cyclic voltammetry

Typically, redox potential, heterogeneous electron transfer rate, and chemical kinetics are investigated to characterise a molecularly defined electrocatalyst. Cyclic voltammetry (CV) is the most frequently used electroanalytical method for such yardstick purposes

besides it can be a useful tool for studying mechanistic aspects (Benson *et al.*, 2009; Francke *et al.*, 2018). Under a dry inert atmosphere, an electrocatalyst should show a reversible redox couple. Upon addition of CO_2, the diffusion-limited current should increase significantly. While the potential shifts anodically, the reversibility in the return oxidation wave is lost due to the chemical reaction between CO_2 and the electrocatalyst.

2.7 Summary

Regardless of the comprehensive research works, scientists are still struggling to design an optimum electrocatalyst for CO_2 reduction as discussed with evidence over the decades. It was found that very minimal studies carried out for multinuclear metal clusters for this purpose that rises to the niche of this research project. The literature above supported that Ni and Co complexes are promising candidates for the design of high-performance catalysts for CO_2 reduction. They hold accessible multiple redox states that can facilitate the electron or/and proton transfer.

Furthermore, electron shuttling via electron reservoir behaviour by the redox-active ligands enhance the selectivity and efficiency besides reducing the overpotential. Thus, the cooperation of redox-active ligand with Co and Ni can be an effective metal complex system for CO_2 reduction.

CHAPTER 3: MATERIALS AND RESEARCH METHODOLOGY

3.1 Introduction

This chapter will discuss the synthesis and characterisation of redox-active ligand, 3,6-di(pyrozol-1-yl)-pyridazine, **L1**, the synthesis method of novel $[Ni_2(C_{10}H_8N_6)_2(CH_3CN)_4](PF_6)_4$, (**1**), $[Ni_4(C_{10}H_8N_6)_4(\mu\text{-}OH)_4](ClO_4)_4$, (**2**) and $[Co_4(C_{10}H_8N_6)_4(\mu\text{-}CH_3O)_2(\mu\text{-}O)_2](PF_6)_3(NO_3)$, (**3**), their purity and the sources. The details of the used instrument and equipment are described further below.

3.2 Materials and chemicals

All chemicals are commercially available and analytical grade, unless otherwise specified. All the reagents were of the highest quality available and were used as received, unless otherwise stated.

Table 3.1: List of chemicals used.

No.	Chemicals & reagents	Purity (%)	Supplier
1	3,6-dichloropyridazine	≥ 98.0	Tokyo Chemical Industry (TCI)
2	Pyrazole	≥ 98.0	TCI
3	Sodium hydride (dispersion in paraffin liquid)	55 – 60	TCI
4	1,8-diazabicyclo [5.4.0]-7-undecene	≥ 98.0	TCI
5	Nickel(II) perchlorate hexahydrate, $Ni(ClO_4)_2.6H_2O$	≥ 98.0	Sigma Aldrich
6	Cobalt(II) nitrate hexahydrate, $Co(NO_3)_2.6H_2O$	≥ 98.0	Sigma Aldrich
8	Sodium hexafluorophosphate, $NaPF_6$	≥ 98.0	Sigma Aldrich
9	*N,N*-dimethylformamide	Dry	Wako Pure Chemical Industries
10	Methanol	> 99.8	Wako Pure Chemical Industries
11	Acetonitrile	HPLC grade	Wako Pure Chemical Industries

Table 3.2,continued.

12	Diethyl ether	HPLC grade	Wako Pure Chemical Industries

3.3 Characterisation

^{1}H-NMR and ^{13}C-NMR spectra were collected at room temperature on a JEOL JNM-ECS400 spectrometer. UV-vis absorption spectra were measured on a Shimadzu UV-2450SIM spectrophotometer at room temperature. Elemental analyses were performed on a J-Science Lab Micro Corder JM10 elemental analyser. Crystals of complex **1**, **2,** and **3** were mounted in a loop. Diffraction data at 123 K were measured on a RAXIS-RAPID Imaging Plate diffractometer equipped with confocal monochromated Mo-Kα radiation and data was processed using RAPID-AUTO (Rigaku). Progress of all the reactions was monitored using thin-layer chromatography (TLC), which was performed on aluminum sheets, precoated with silica gel (Merck, Kiselgel 60 F-254) (0.2 mm). Electrochemical activity was analysed with BAS ALS Model 650DKMP electrochemical analyser.

3.3.1 Fourier transform infrared (FTIR)

The functional groups analysis of **L1** and synthesised metal clusters were measured using an attenuated total reflection FTIR Spectrometer (Thermo Nicolet 6700, Waltham, United States). The FTIR was performed in the wavenumber range of 500 cm^{-1} to 4000 cm^{-1}. The spectra were recorded with a resolution of 4 cm^{-1} with 32 scans. The baseline of spectra was corrected.

3.3.2 Proton nuclear magnetic resonance (^{1}H NMR)

L1 was dissolved in deuterated chloroform ($CDCl_3$-*d*) (99.8%) (Sigma Aldrich) solvents. Diamagnetic metal clusters were measured with deuterated N-N-dimethylformamide (DMF-d_7) and acetonitrile (CD_3CN-d_3). The ^{1}H NMR spectra were

acquired using JEOL JNM-ECS400 spectrometer (JEOL USA.Inc) at 400 MHz. Each sample was accumulated at 16 scans. Chemical shifts reported in ppm on the δ scale were calibrated on the solvent peak and referenced to internal tetramethylsilane (TMS) unless specified.

3.3.3 Carbon-13 nuclear magnetic resonance (^{13}C NMR)

The ^{13}C NMR spectra were acquired using JEOL JNM-ECS400 spectrometer (JEOL USA.Inc) at 400 MHz. Each sample was analysed at 1000 scans. Chemical shifts reported in ppm on the δ scale were calibrated on the solvent peak and referenced to internal tetramethylsilane (TMS) unless specified.

3.3.4 Single-crystal X-ray diffraction (SCXRD)

The structure of complexes **1** and **3** was solved by Intrinsic Phasing using *SHELXT* (Sheldrick, 2015b) structure solution program with *Olex2* (Dolomanov *et al.*, 2009) and refined by the Least Squares minimisation techniques on *SHELXL* (Sheldrick, 2015a). The structure of complex **2** was solved by Direct Method using *SIR92* (Altomare *et al.*, 1994) and refined by the least-squares against F^2 using the SHELXL-2018/3 package (Sheldrick, 2015b). All non-hydrogen atoms were refined anisotropically. For complex **2,** the diffused electron densities resulting from the residual solvent molecules were removed from the data set using the SQUEEZE routine of PLATON (Read, & Kleywegt, 2009) and refined further using the generated data. Crystallographic data have been deposited with Cambridge Crystallographic Data Centre: Deposition number CCDC for complexes **1, 2** and **3**: 1901925, 1901926 and 1904602 respectively. Copies of the data can be obtained free of charge via www.ccdc.cam.ac.uk/data_request/cif.

3.3.5 Cyclic voltammetry analysis

Electrochemical experiments were performed at room temperature under inert and CO_2 environment on a BAS ALS Model 650DKMP electrochemical analyser. The analyte

concentration was measured at 0.5 mM in 2mL of N-N-dimethylformamide with a 0.1 M tetrabutylammonium perchlorate (TBAP) as the electrolyte. CV was performed by using a one-compartment cell with a three-electrode configuration, which consisted of a glassy carbon working electrode (diameter = 3mm), Pt-wire auxiliary electrode, and Ag/Ag^+ electrode (Ag/0.01 M $AgNO_3$) reference electrode. The redox potentials were calibrated against the redox potential for the ferrocene/ferrocenium (Fc/Fc^+) couple which was found at ~0.15 V vs. Ag/Ag^+ in N-N-dimethylformamide. The glassy carbon disc working electrode was polished using alumina prior to each measurement. The concentration of CO_2 during the measurements was controlled using KOFLOC RK1200M and 8500MC-0-1-1 flow meter.

(a) ***Details of typical CV experiments***

The identification of electrocatalytic activity can be seen easily in cyclic voltammetry (Figure 3.1). Step 1*:* The voltammetry experiment should first be carried out under inert atmosphere (N_2) to determine the reduction potential E^0_{cat} and the cathodic peak current i_p of the catalyst (**curve 1**). This reversibility is generally preferred but not a mandatory requirement. Nevertheless, point to concern in this situation there is always a kinetic competition between the reaction making the redox couple irreversible and the reaction with CO_2 (Francke *et al.*, 2018).

Step 2: When the potential has been estimated in the appropriate range, the solution can be saturated with CO_2 and the measurement be repeated. When the conditions mentioned above are optimised, a catalytic current ($i_{cat} > i_P$) is now observed (**curve 2**). At this moment, the reversible shape of the CV (**curve 1**) often changes to the irreversible form indicated with **curve 2**. The shape of this CV results from competition between the consumption of CO_2 by the rate-determining step of the catalytic cycle with a diffusion of the fresh substrate to the electrode.

Step 3: An overlap between direct and indirect CO_2 reduction as well as with cathodic decomposition of electrolyte is not desirable, to examine this possibility, the voltammetry response of the blank electrolyte under N_2 (**curve 3**) and CO_2 (**curve 4**) should also be known.

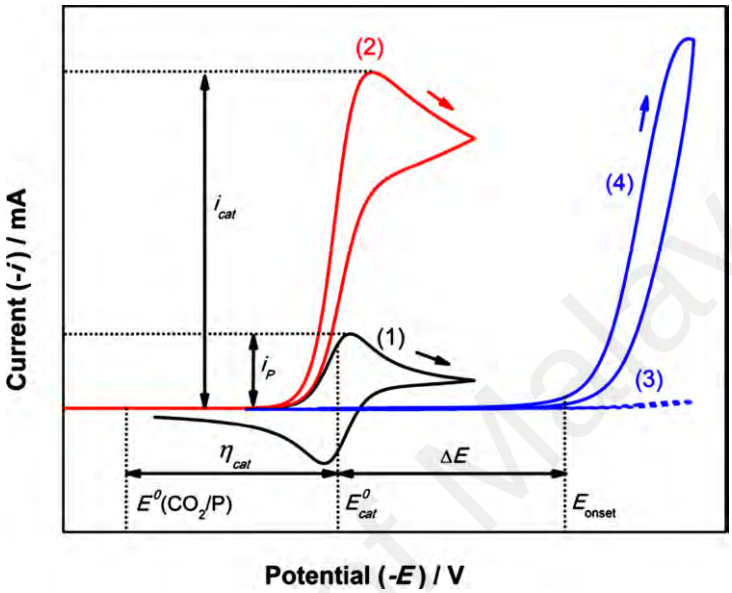

Figure 3.1: Schematic illustration of the voltammetric analysis of the electrocatalytic CO_2 reduction. (1) Voltammetry of the catalyst under N_2 atmosphere. (2) Catalyst, CO_2 atmosphere. Under a CO_2 environment is readily observed: (a) Anodic potential shift, (b) large increase in current, (c) non-reversible waveform. (3) Blank electrolyte, N_2 atmosphere. (4) Blank electrolyte, CO_2 atmosphere. (Francke *et al.*, 2018).

3.3.6 Controlled-potential electrolysis

Controlled-potential electrolysis was performed in a gas-tight two-compartment electrochemical cell. The first compartment held the carbon plate working electrode (1.2 cm^2 surface area) and a leak less Ag/AgCl reference electrode in DMF containing 0.1 M TBAP (5 ml) with 0.5 mM complexes, while the second compartment held the Pt auxiliary electrode containing 0.1 M TBAP/DMF (5 ml) containing ferrocene (40 mM) as a sacrificial reductant. The two compartments were separated by Nafion® membrane. The solution was purged vigorously with CO_2 for 30 mins prior to electrolysis. The

electrolysis experiment was performed for 1 h under constant stirring. The amount of CO and H_2 produced at the headspace of the cell was quantified with Shimadzu GC-8A with TCD detector equipped with capillary column with Molecular Sieve 13X-S 60/80. On the other hand, the liquid product was quantified by using Shimadzu LC-20AD with SPD-2 and RID-10A detectors equipped with Shim-pack SCR102H column. A calibration curve was made by sampling known amounts of H_2 and CO and HCOOH.

3.4 Syntheses

3.4.1 Synthesis of 3,6-bis(pyrazol-1-yl)pyridazine, (L1)

A mixture of pyrazole (170.20 mg, 2.5 mmol) and sodium hydride 55% (110.00 mg, 2.5 mmol) was stirred in N-N-dimethylformamide for one hour under inert atmosphere. After that, 3,6-dichloropyridazine (148.97 mg, 1.0 mmol) in N-N-dimethylformamide was added dropwise to the reaction mixture which was placed in an ice bath. It was then stirred in an ice bath for an hour and 12 hours under room temperature. Reaction progress was monitored with TLC (n-hexane/ethyl acetate (1:1 (v/v)). 40 mL of ice water was added to the reaction mixture and a white precipitate was formed immediately. The precipitate was filtered under vacuum and washed with minimal amount of cold water. The product formed was dried under vacuum. Yield: 182.7 mg, (96%).

3.4.2 Syntheses of complexes

Syntheses of complexes **1, 2,** and **3** were carried out according to the literature (Okamura *et al.*, 2016) with slight modifications.

3.4.2.1 $[Ni_2(C_{10}H_8N_6)_2(CH_3CN)_4](PF_6)_4$, (1)

L1 (21.21 mg, 0.1 mmol) was dissolved in 10 mL chloroform and was added dropwise to the nickel(II) perchlorate hexahydrate, $Ni(ClO_4)_2{\bullet}6H_2O$ (73.14 mg, 0.2 mmol) which pre-dissolved in 5 mL methanolic solution. Lavender coloured cloudy mixture was formed immediately. The reaction mixture was stirred for 30 mins at room temperature

and was concentrated under vacuum. A minimum amount of acetonitrile was added to dissolve the precipitate. A concentrated aqueous solution of sodium hexafluorophosphate, $NaPF_6$ (5 equiv.) was added to the acetonitrile mixture and acetonitrile was removed completely under pressure at 40 ^oC. The mixture was filtered under vacuum and washed with minimum amount of cold water. The lavender coloured crystals of **1** were grown by vapour diffusion technique from acetonitrile/diethyl ether solution. Yield: 101.0 mg (75.3%).

3.4.2.2 $[Ni_4(C_{10}H_8N_6)_4(\mu\text{-}OH)_4](ClO_4)_4$, (2)

L1 (21.21 mg, 0.1 mmol) was dissolved in 10 mL chloroform and 1,8-diazabicyclo[5.4.0]undec-7-ene (DBU) (14.95 µL, 0.1 mmol) was added dropwise. The ligand mixture was added dropwise to the nickel(II) perchlorate hexahydrate, $Ni(ClO_4)_2{\bullet}6H_2O$ (73.14 mg, 0.2 mmol) in 5 mL acetone solution. Light green turquoise cloudy mixture was formed immediately. The reaction mixture was stirred for 30 mins at room temperature. The precipitate was filtered under vacuum filtration and washed with cold water. After dried under air, **2** was obtained as purple powder. Violet coloured crystals of **2** were grown by vapour diffusion technique from acetonitrile/diethyl ether solution. Yield: 61.0 mg (38.1%).

3.4.2.3 $[Co_4(C_{10}H_8N_6)_4(\mu\text{-}CH_3O)_2(\mu\text{-}O)_2](PF_6)_3(NO_3)$, (3)

L1 (21.21 mg, 0.1 mmol) was dissolved in 10 mL chloroform and 1,8-diazabicyclo[5.4.0]undec-7-ene (DBU) (14.95 µL, 0.1 mmol) was added dropwise. The ligand mixture was added dropwise to the cobalt(II) nitrate hexahydrate, $Co(NO_3)_2{\bullet}6H_2O$ (36.59 mg, 0.2 mmol) in 5 mL methanol solution. Dark red cloudy mixture formed immediately. The reaction mixture was stirred at least for 30 mins at room temperature. Concentrated sodium hexafluorophosphate, $NaPF_6$ (5 equiv.) was added to the acetonitrile mixture and acetonitrile removed completely under pressure at 40 ^oC. The mixture was

filtered under vacuum and washed with minimal amount of cold water, chloroform, and diethyl ether. After dried under air, **3** was obtained as dark orange red. Dark orange red coloured crystal of **3** was grown by vapour diffusion technique from acetonitrile/diethyl ether solution. Yield: 45.3 mg (27.0%).

CHAPTER 4: RESULTS AND DISCUSSION

4.1 Introduction

In this work, one neutral N6-ligand was prepared by substitution reaction of 3,6-dichloropyridazine and pyrazole in 1:2 mole ratio in the presence of a strong base. **L1** was synthesised according to the literature procedures (Anthony W. Addison, 1981; Ather *et al.*, 2013; Steiner *et al.*, 1981) with modifications. The reaction equation is shown in Scheme 4.1.

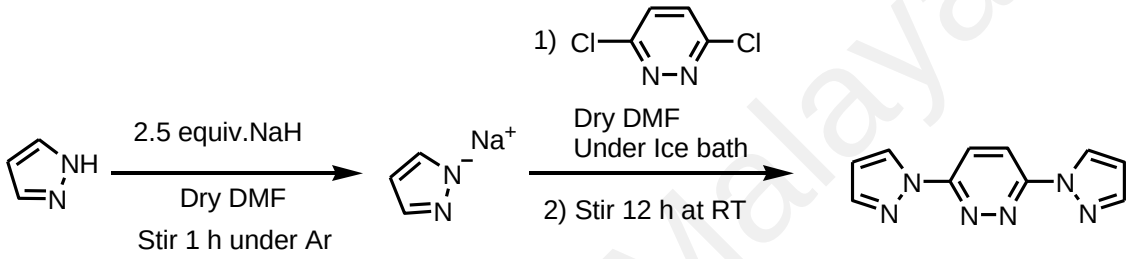

Scheme 4.1: Synthesis of **L1**.

The **L1** was reacted with Ni(II) and Co(II) salts according to the literature (Okamura *et al.*, 2016) with slight modifications. Attempt to make multinuclear metal complexes with the presence of base was successful that confirmed by single-crystal X-ray analysis. These metal ions were chosen because Ni(II) has been utilised by nature's catalytic system (Jeoung, & Dobbek, 2007) and Co(II) as an efficient metal for CO_2 reduction (Francke *et al.*, 2018).

L1 acts as in a tetradentate manner coordinating through pyridazinyl and pyrazolyl nitrogen yielded dinuclear Ni(II) complex, **1**, tetranuclear Ni(II) complex, **2**, and tetranuclear Co(II/III) complex, **3**. This is the very first successful attempt of synthesising multinuclear transition metal complex utilising **L1** ligand (Gupta *et al.*, 2009; Gupta *et al.*, 2010; Sangilipandi *et al.*, 2015). Tetranuclear complex **2** and **3** were selectively produced in the presence of base, while dinuclear complex **1** was obtained in the absence

of base. Under basic conditions with the coordinating solvent, hydroxyl ions play an important role as the bridging ligand to form the tetranuclear complex. The general synthetic route of the multinuclear pyrazolyl pyridazine complexes of dinuclear and tetranuclear Ni and Co are presented in Scheme 4.2.

The chemical and structural characterisation of the ligand was confirmed by FTIR, elemental analyses, ^{1}H-NMR, and ^{13}C-NMR and its electronic property by UV-vis spectroscopy. Metal complexes were analysed with elemental analyses, FTIR and single-crystal X-ray analysis. Their electrochemical properties were analysed by cyclic voltammetry and controlled potential electrolysis.

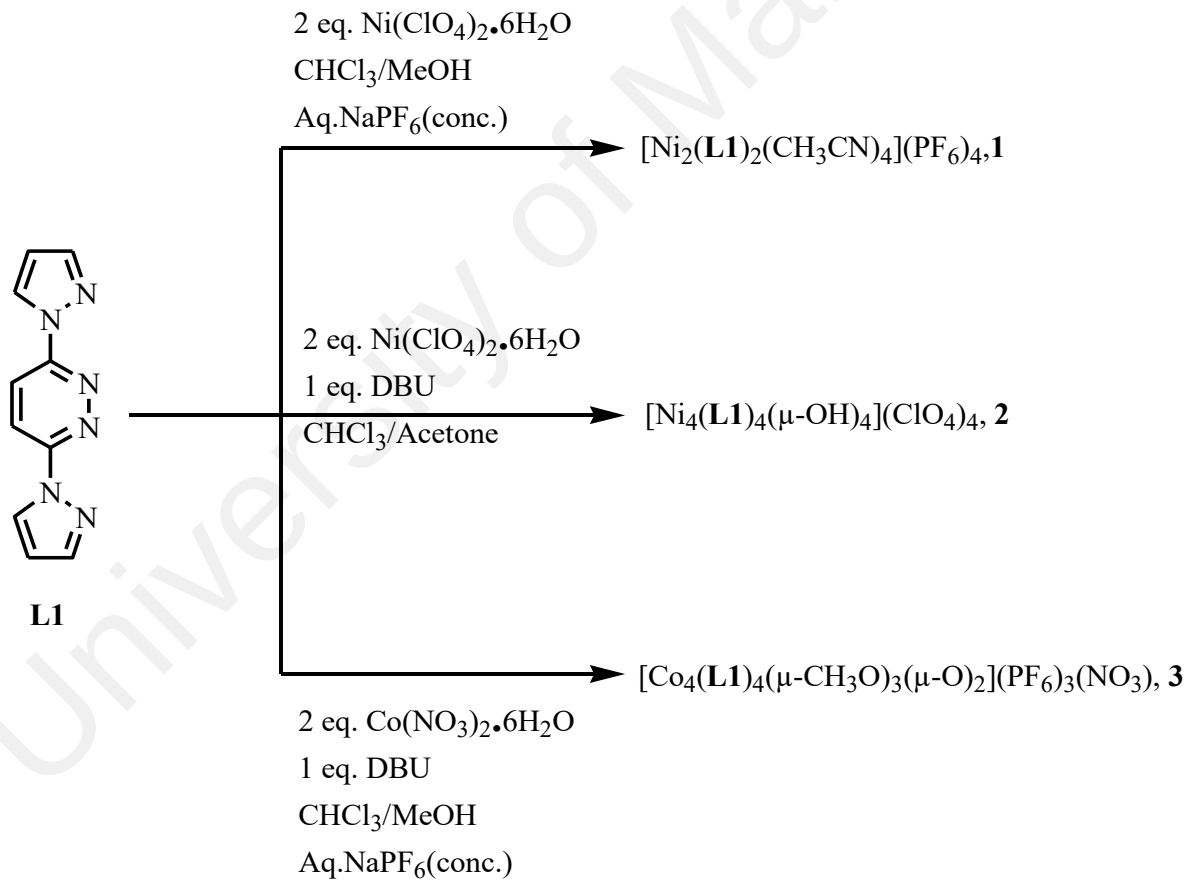

Scheme 4.2: Synthesis route of metal complexes **1**, **2**, and **3**.

4.2 Elemental analyses

Figure 4.1 shows the structure of 3,6-bis(pyrazol-1-yl)pyridazine, **L1**. It was obtained as a white powder in an exceptional yield (96%) from the reaction shown in Scheme 2.1. The results from C, H, N elemental analyses were in excellent agreement with the expected empirical formula $C_{10}N_6H_8$. Elemental analyses: Found: C,56.40; H,3.70; N,39.70. Calc. or $C_{10}H_8N_6$: C,56.60; H,3.80; N,39.60%.

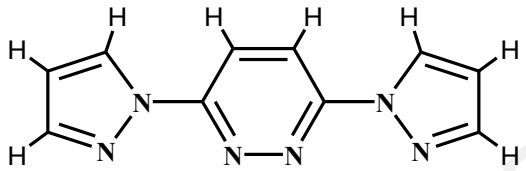

Figure 4.1: 3,6-bis(pyrazol-1-yl)pyridazine, **L1**.

4.2.1 $[Ni_2(C_{10}H_8N_6)_2(CH_3CN)_4](PF_6)_4$, (1)

L1 was reacted with nickel(II) perchlorate hexahydrate, $Ni(ClO_4)_2 \cdot 6H_2O$ in mole ratio of 1:2, to produce a lavender crystal, complex **1** and the yield was 75.3%. The counter anion perchlorate (ClO_4^-) was exchanged with hexafluorophosphate (PF_6^-) to obtain a higher quality single crystal. It was readily soluble in *N,N*-dimethylformamide and dimethylacetamide but not in other common polar or non-polar solvents. The result from C, H, N elemental analyses for complex **1**: Found: C,24.80; H,2.82; N,16.60. Calc. for $[Ni_2(C_{10}H_8N_6)_2(CH_3CN)_4](PF_6)_4 \bullet 3H_2O$: C,24.77; H,2.67; N,16.50%. Formula weight of **1** is 1285.87 $gmol^{-1}$.

4.2.2 $[Ni_4(C_{10}H_8N_6)_4(\mu\text{-}OH)_4](ClO_4)_4$, (2)

L1 was reacted with nickel(II) perchlorate hexahydrate, $Ni(ClO_4)_2 \cdot 6H_2O$ in mole ratio of 1:2 in the presence of base, DBU to produce a violet crystal, complex **2** and the yield was moderate (38.1%). The yield is low due to a possible mixture of mononuclear and dinuclear complex formation during the metal complexation process. It was readily

soluble only in *N,N*-dimethylformamide. The result from C, H, N elemental analyses for complex **2**: Found: C,30.40; H,2.34; N,21.10. Calc. for $[Ni_4(C_{10}H_8N_6)_4(\mu\text{-}OH)_4](ClO_4)_4 \bullet 3H_2O$: C,30.43; H,2.81; N,20.77%. Formula weight of **2** is 1600.52 $gmol^{-1}$.

4.2.3 $[Co_4(C_{10}H_8N_6)_4(\mu\text{-}CH_3O)_2(\mu\text{-}O)_2](PF_6)_3(NO_3)$, (3)

L1 was reacted with cobalt(II) nitrate hexahydrate, $Co(NO_3)_2 \cdot 6H_2O$ in mole ratio of 1:2 in the presence of base, DBU to produce a dark red orange crystal, **3** and the yield was moderate (30.4%). The yield is low due to a possible mixture of mononuclear and dinuclear complex formation during the metal complexation process. It was readily soluble only in acetonitrile, and *N,N*-dimethylformamide. The result from C, H, N elemental analyses for complex **3**: Found: C,31.60; H,2.34; N,20.50. Calc. for $[Co_4(C_{10}H_8N_6)_4(\mu\text{-}O)_2(\mu\text{-}OCH_3](PF_6)_3(NO_3)$: C,31.70; H,2.54; N,20.64%. Formula weight of **3** is 1628.57 $gmol^{-1}$.

Table 4.1: Elemental analyses of **L1** and complexes **1-3**.

Ligand/Metal complexes	Elemental analyses (C,H,N) (%)	
	Calculated	Found
L1	C:56.40 H:3.70 N:39.70	C:56.60 H:3.80 N:39.60
Complex **1**	C:24.77 H:2.67 N:16.50	C:24.80 H:2.82 N:16.60
Complex **2**	C:30.43 H:2.81 N:20.77	C:30.40 H:2.34 N:21.10
Complex **3**	C:31.70 H:2.54 N:20.64	C:31.60 H:2.34 N:20.50

4.3 UV-Vis spectroscopy analysis

The electronic spectrum of a colourless solution of **L1** in $CHCl_3$ as shown in Figure 4.2 demonstrates high-energy absorption at 280 nm (ε = 349.8 $M^{-1}cm^{-1}$). This band was attributed to $\pi \rightarrow \pi^*$ transition of the aromatic ring due to the ligand to ligand charge transfer (LLCT) and intra-ligand (IL) (Sangilipandi *et al.*, 2015). Gupta and co-workers reported pyrazolyl pyridazine ligand display a ligand-based $\pi \rightarrow \pi^*$ transition in UV region that is agreeable with the **L1** band in the UV region. (Dai *et al.*, 2009; Gupta *et al.*, 2010; Sangilipandi *et al.*, 2015).

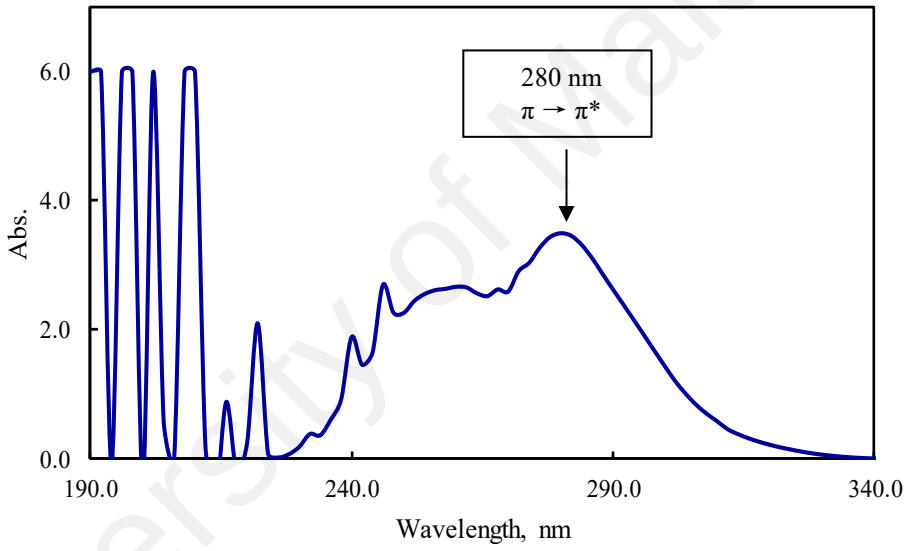

Figure 4.2: UV-Vis spectrum of **L1** in $CHCl_3$

4.4 FTIR spectroscopy analyses

The recorded FTIR spectrum of **L1** is shown in Figure 4.3 The absence of N-H absorption band of pyrazole in the spectrum indicated the formation of **L1**. The spectrum shows the characteristic of strong peak due to the aromatic N=N stretching at 1452 cm^{-1}, medium absorption band attributed to aromatic C=N stretching at 1582 cm^{-1} (Zhu, & Holliday, 2010)(Zhu, & Holliday, 2010)(Zhu, & Holliday, 2010)(Zhu, & Holliday, 2010)(Zhu, & Holliday, 2010)(Zhu & Holliday, 2010). Other than these, peak bands in

the region 3102 – 3150 cm^{-1} were assigned to aromatic C-H stretching while in the region 1000 – 1500 cm^{-1} were assigned to aromatic C-H vibrations.

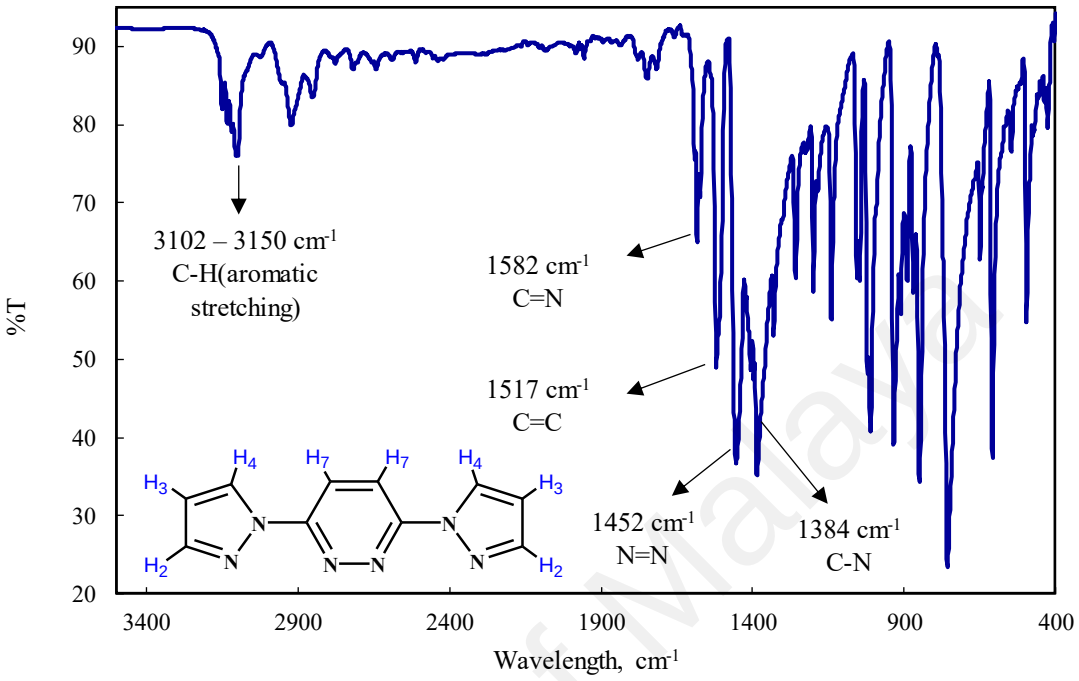

Figure 4.3: FTIR spectrum of **L1**.

The FTIR spectra of complex **1-3** are shown below (Figure 4.4 -Figure 4.6). The strong absorption band of N=N stretching band shifted from 1452 to (1493-1489) cm^{-1} for the complexes as compared to the free ligand. The complexes spectra show the ligand characteristic medium absorption band at the range 1590 - 1599 cm^{-1} and strong absorption band 1406 - 1396 cm^{-1} due to C=N stretching and C-N stretching, respectively. Gupta et.al reported similar phenomena in their complexes bearing **L1** as well.

The spectrum shows a characteristic weak absorption band due to acetonitrile C≡N stretching at 2289 cm^{-1} and the sp^3 C-H stretching at 3145 cm^{-1} indicates the presence of acetonitrile in the complex **1**. However, bridging ligand for complex **2** showed a broad peak band at 3546 cm^{-1} was assigned to O-H stretching of a hydroxy bridging ligand. Complex **3** demonstrated a strong peak at 1353 cm^{-1} and 1048 cm^{-1} were assigned to N-

O stretching of nitrate counter anion and C-O stretching respectively. This indicates the presence of methoxy group bonded to Co(II) centre.

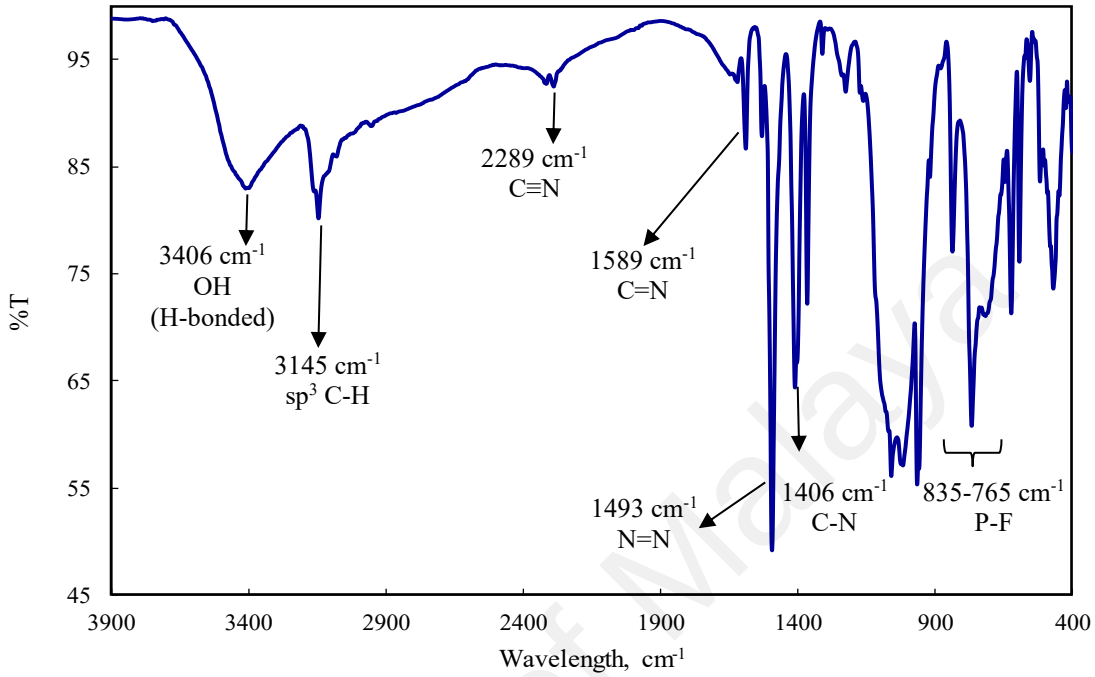

Figure 4.4: FTIR spectrum of complex **1**.

Counter ion PF_6 for complex **1** and **3** demonstrated strong peaks in the region 822 – 758 cm^{-1} due to P-F vibrations in the complexes (Gupta *et al.*, 2010). As for Complex **2** strong peaks observed in the region 1071 - 951 cm^{-1} which were assigned to the stretching of the perchlorate ion as the counter ions (Gupta *et al.*, 2009; Nakamoto, 1988).

Other than these, weak peak band at 3645 – 3406 cm^{-1} was due to O-H stretching of water molecule, 3145 cm^{-1} due to sp^3 C-H stretching frequency and 3125 cm^{-1} due to aromatic C-H. Table 4.2 summarises FTIR data of **L1** and complexes **1-3**.

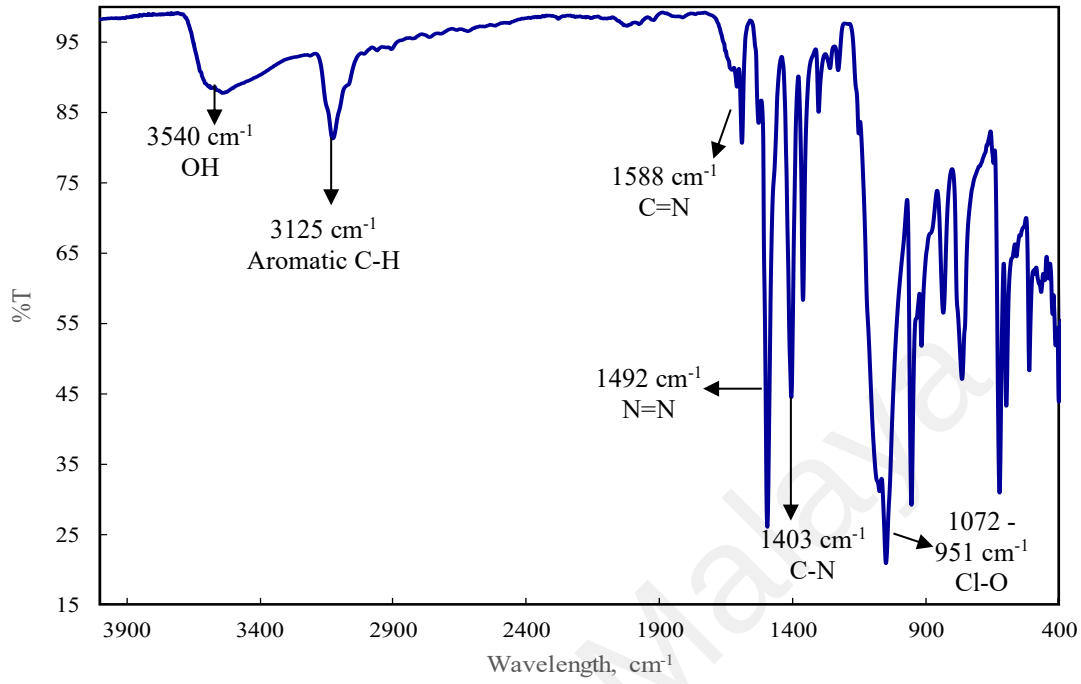

Figure 4.5: FTIR spectrum of complex **2**.

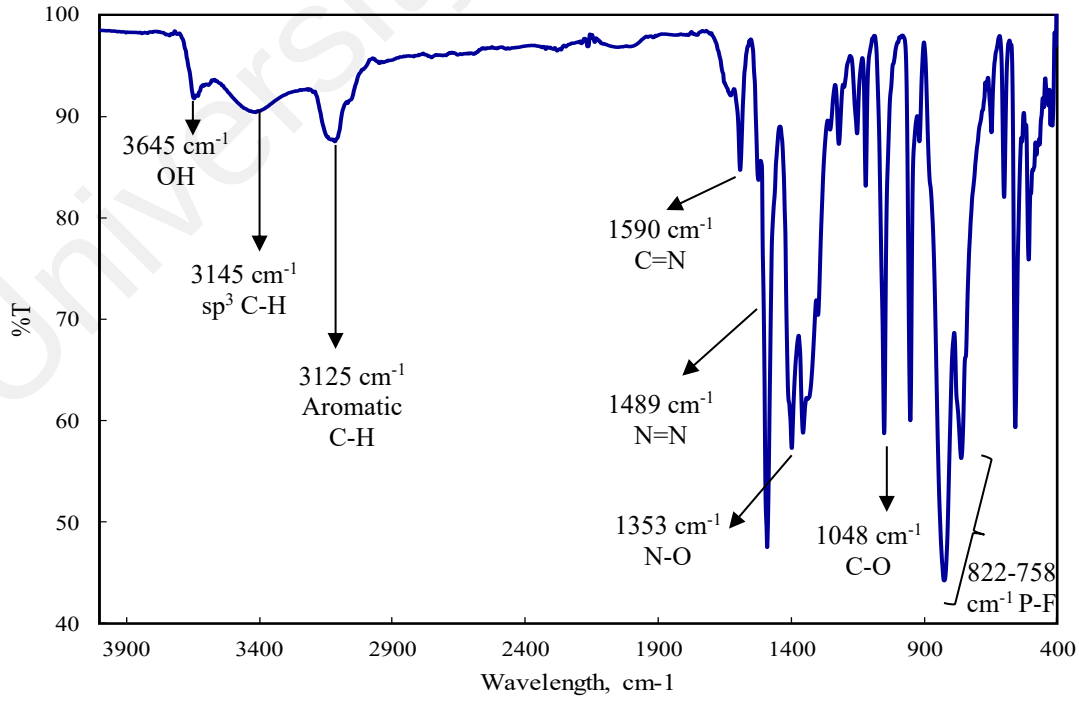

Figure 4.6: FTIR spectrum of complex **3**.

Table 4.2: FTIR data for **L1** and complexes **1-3**.

Type of bond	Wavenumber, ν (cm-1)			
	L1	**Complex 1**	**Complex 2**	**Complex 3**
O-H	-	3406,(b,s)	3540,(b,s)	3645,(w)
sp3 C-H	-	3145,(m)	-	3147,(w)
C-H (aromatic stretching)	3102-3150,(m)	-	3125,(w)	3125,(w)
C≡N	-	2289,(w)	-	-
C=N	1582,(m)	1589	1588,(m)	1590,(m)
C=C	1517,(s)	-	-	-
N=N	1452,(s)	1493,(s)	1492,(s)	1489,(s)
C-N	1384,(s)	1406,(s)	1403,(s)	1396,(s)
N-O	-	-	--	1353,(s)
C-O	-	-		1048,(s)
Cl-O	-	-	1071 – 951,(s)	-
P-F	-	835-765,(s)		822-758,(s)

[a] *b:* broad, *s:* strong, *m:* medium, *w:* weak

4.5 Nuclear magnetic resonance spectroscopy analyses

The ^{1}H-NMR of **L1** was recorded as a solution in $CDCl_3$-*d* is shown in Figure 4.7. The assignments of the spectrum are consistent with the expected structure of **L1**: a singlet at 8.35 ppm is due to two same environments aromatic proton (H_3) of pyridazine ring. Ather and co-workers reported a singlet peak at 8.75 ppm assigned to pyridazine ring were analysed with trifluoroacetic acid (Ather *et al.*, 2013). A doublet at 8.73 ppm is due to aromatic proton (H_2) located near nitrogen of pyrazole ring, a doublet at 7.81 ppm is due to aromatic proton (H_4) of pyrazole ring which located near pyridazine ring, and a doublet

of a doublet at 6.55 ppm is due to aromatic proton (H_7) situated in between of H_2 and H_7 of pyrazole ring. The integration ratio for the protons H_2:H_3:H_4:H_7 is 1:1:1:1, respectively.

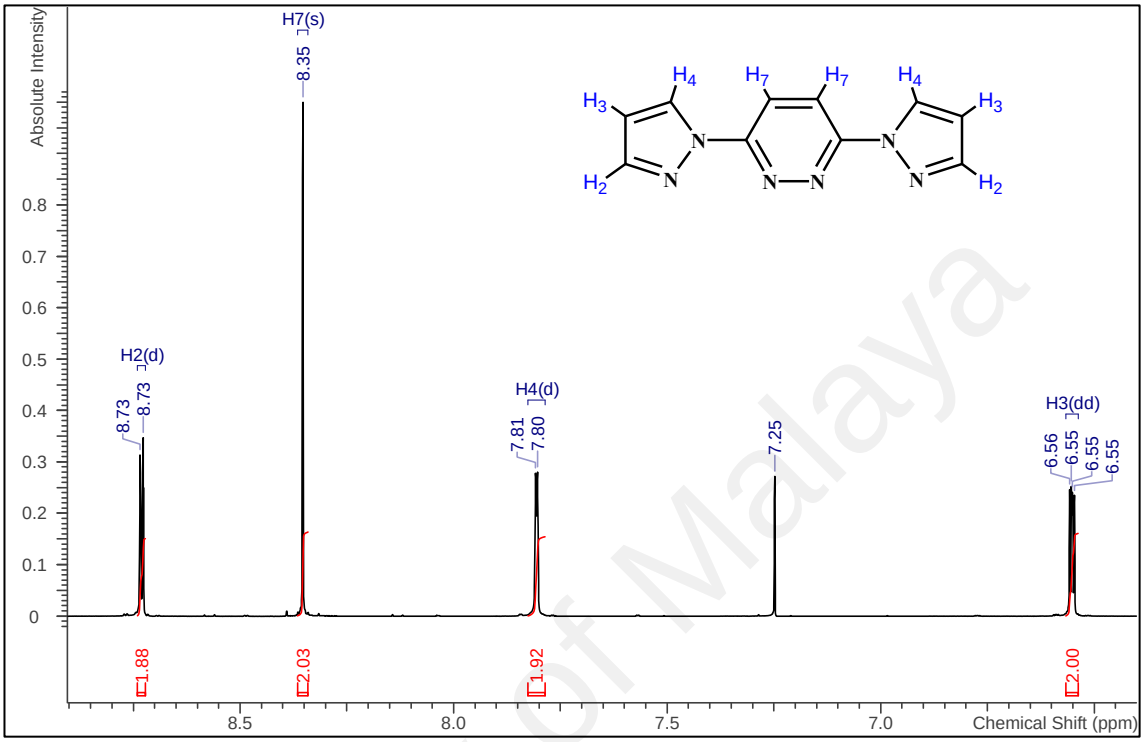

Figure 4.7: ^{1}H-NMR spectrum of **L1**.

The ^{13}C-NMR of L1 was recorded as a solution in $CDCl_3$-*d* is shown in Figure 4.8. The spectrum indicated the presence of five carbons located at the heteroaromatic compound chemical shift region which agrees with the molecular formula of L1. The signals at 127.2, 109.0, and 143.0 ppm in the downfield region were attributed to carbons of pyrazole ring. The spectrum showed absorption peaks at 127.0 ppm, and 109.0 ppm which were due to C_2 and C_3 of the pyrazole ring, respectively. A strong absorption peak at 143.0 ppm was assigned to C_4 of the pyrazole ring. Meanwhile, signals at 154.0 and 120.5 ppm in the downfield region were attributed to the pyridazine ring. A very low intensity absorption peak at 154.0 ppm was assigned to C_6 of pyridazine ring whereas strong absorption peak at 120.5 ppm was assigned to C_7 of the pyridazine ring.

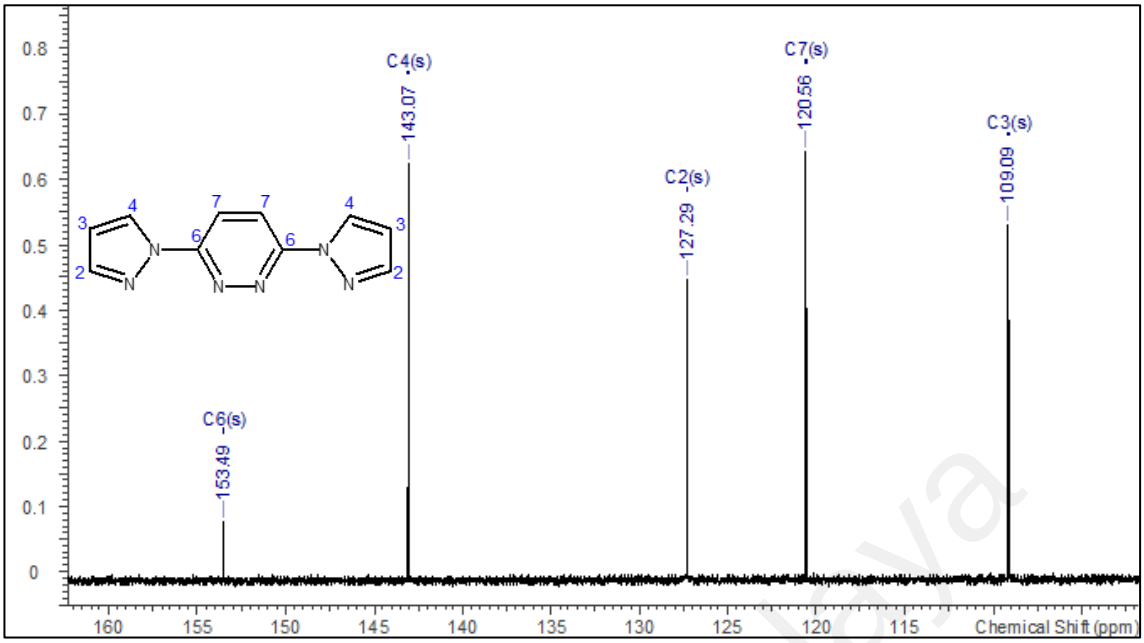

Figure 4.8: ^{13}C-NMR spectrum of **L1**.

^{1}H-NMR and ^{13}C-NMR data of L1 agreed with the proposed structure. Table 4.3 shows summarised ^{1}H-NMR and ^{13}C-NMR data of **L1**. **L1** is a known ligand and structural characterisation has reported. Comparatively, the reported structure observed to show similar splitting and chemical shifts for each proton and carbon too (Ather *et al.*, 2013; Dai *et al.*, 2009).

Table 4.3: ^{1}H-NMR & ^{13}C-NMR data of **L1**.

Proton/carbon assignments	Chemical shift, δ (ppm)[a]	
	^{1}H-NMR	**^{13}C-NMR**
2	8.73 (d, 2H)	127.2
3	6.55 (dd, 2H)	109.0
4	7.81 (d, 2H)	143.0
6	-	154.0
7	8.35 (s, 2H)	120.5

[a] d: doublet; s: singlet; dd: doublet of double

4.6 Crystal structure analyses

Crystallisation of complex **1** by vapour diffusion technique from acetonitrile/diethyl ether solvent system formed lavender coloured crystal which was analysed by X-ray diffraction. X-ray crystal structure analysis revealed that the complex was centrosymmetric and adopted a slightly distorted octahedral geometry. Complex **1** was crystallised in monoclinic *C*2/*c* space group. The asymmetric unit and coordination environment of Ni atom was shown in Figure 4.9 and Figure 4.10. The central Ni atoms were surrounded octahedrally by two neutral tetradentate ligands in a *trans*-isomer arrangement and two acetonitrile molecules. Each Ni atom was coordinated with four nitrogen atoms (N1, N3, N4, N6) of two L1 ligands and two nitrogen atoms (N7, N8) of two acetonitrile. Due to the small bite angle of the structure of the ligand, the octahedral coordination spheres of the central Ni atoms were slightly distorted. The crystal system and refinement data were shown in Table 4.4. Selected bond lengths were shown in Table 4.5.

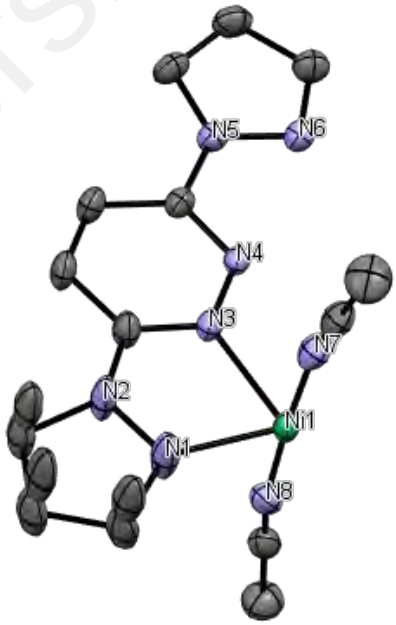

Figure 4.9: Asymmetric X-ray crystal structure of complex **1**,$[Ni_2(C_{10}H_8N_6)_2(CH_3CN)_4](PF_6)_4$ with thermal ellipsoids (50% probability). Hydrogen atoms and the four PF_6 anions have been omitted for clarity.

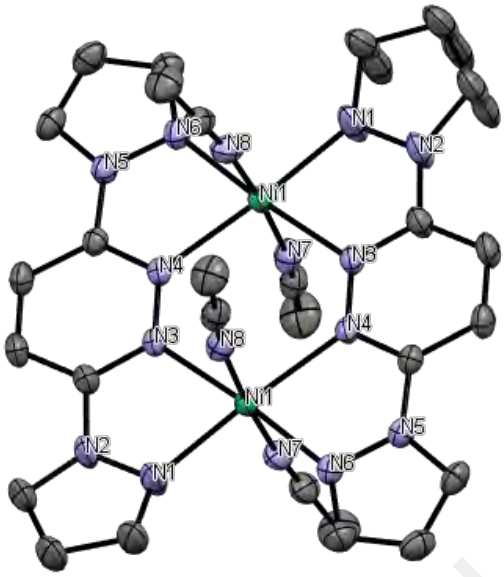

Figure 4.10: Overall X-ray crystal structure of complex **1**, $[Ni_2(C_{10}H_8N_6)_2(CH_3CN)_4](PF_6)_4$ with thermal ellipsoids (50% probability). Hydrogen atoms and the four PF_6 anions have been omitted for clarity.

Table 4.4: Crystal system and refinement data of complex **1**.

Complex	**1**
Empirical formula	$C_{32}H_{34}F_{24}N_{18}Ni_2P_4$
Formula weight	1368.07
Crystal system	monoclinic
Space group	C2/c
a/Å	15.565(5)
b/Å	15.488(5)
c/Å	21.446(5)
α/o	90
β/o	99.892(5)
γ/o	90

Table 4.4, continued.

Volume/Å3	5093(3)
Z	4
ρcalc g/cm3	1.784
μ/mm-1	1.002
F(000)	2736.0
Crystal size/mm3	0.211 x 0.195 x 0.182
Radiation	MoKα (λ = 0.71073)
θ range for data collection	3.856 to 54.97
Reflections collected	25278
Independent reflections	5831[Rint = 0.0212, Rsigma = 0.0181]
Data/restraints/parameters	5831/53/403
Goodness-of-fit on F2	1.096
Final R indices [I > 2σ(I)]	R1 = 0.0711, wR2 = 0.2163
R indices (all data)	R1 = 0.0783, wR2 = 0.2255

Table 4.5: Selected bond lengths (Å) and bond angles (°) of complex **1**.

Bond lengths (Å)		**Bond angles (°)**	
Ni1-N6^{1}	2.057 (3)	N6^{1}-Ni1-N3	175.65 (10)
Ni1-N3	2.116 (3)	N6^{1}-Ni1-N4^{1}	78.10 (11)
Ni1-N4^{1}	2.122 (3)	N6^{1}-Ni1-N8	90.54 (10)
Ni1-N8	2.058 (3)	N6^{1}-Ni1-N7	89.63 (10)
Ni1-N1	2.055 (3)	N3-Ni1-N4^{1}	106.24 (11)
Ni1-N7	2.061 (3)	N8-Ni1-N3	89.97 (9)
Ni1-Ni1	3.885 (1)	N8-Ni1-N4^{1}	87.06 (9)

Table 4.5, continued.

		N8-Ni1-N7	175.78 (11)
		N1-Ni1-N6[1]	97.87 (12)
		N1-Ni1-N3	77.80 (12)
		N1-Ni1-N4[1]	175.96 (11)
		N1-Ni1-N8	92.74 (14)
		N1-Ni1-N7	91.42 (13)
		N7-Ni1-N3	90.18 (10)
		N7-Ni1-N4[1]	88.85 (9)

1-X,+Y,3/2-Z

Crystallisation of complex **2** by vapour diffusion technique from acetonitrile/diethyl ether solvent system formed violet coloured crystal which was analysed by X-ray diffraction. X-ray crystal structure analysis revealed that the complex was centrosymmetric and adopted a slightly distorted octahedral geometry. Complex **2** was crystallised in tetragonal $I4_1/amd$ space group. The asymmetric unit and coordination environment of Ni atom was shown in Figure 4.11 and Figure 4.12 respectively. Each Ni central atom was surrounded octahedrally by two neutral tetradentate ligands in a *cis*-isomer arrangement and bridged by two hydroxide ligands. The bridging ligands formation occurred due to the utilisation of DBU as a base during the complexation process. Each Ni atom was coordinated with four nitrogen atoms (N1, N3) of two **L1** ligands and two oxygen atoms (O1) of hydroxide bridging. Once again, the bulkiness and symmetric characteristic of the ligand, the octahedral coordination spheres of the central Ni atoms were slightly distorted. Two Ni(II) centres were bridged by the ligand to form a twelve-membered macrocycle which adopts a boat configuration. In this type of ring, the four Ni(II) centres were exactly coplanar to present a square configuration (Gao *et al.*,

2006). The crystal system and refinement data were shown in Table 4.6. Selected bond lengths were shown in Table 4.7.

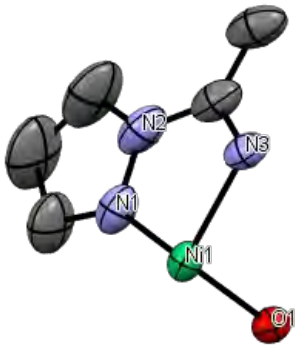

Figure 4.11: Asymmetric X-ray crystal structure of complex **2**, $[Ni_4(C_{10}H_8N_6)_4(\mu\text{-}OH)_4](ClO_4)_4$ with thermal ellipsoids (50% probability). Hydrogen atoms and the four ClO_4 anions have been omitted for clarity.

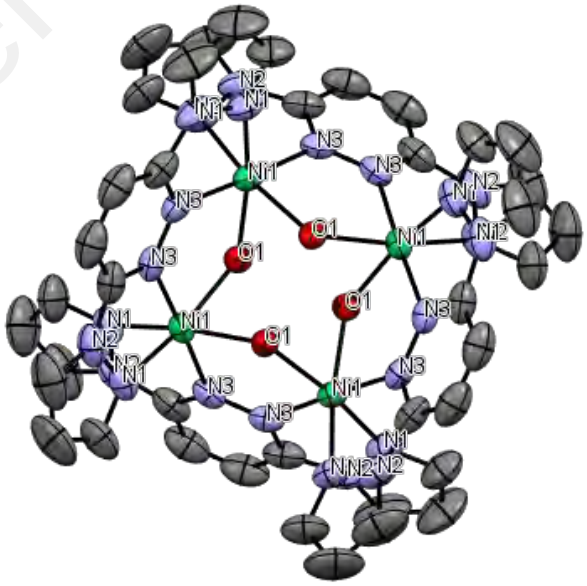

Figure 4.12: Overall X-ray crystal structure of complex **2**, $[Ni_4(C_{10}H_8N_6)_4(\mu\text{-}OH)_4](ClO_4)_4$ with thermal ellipsoids (50% probability). Hydrogen atoms and the four ClO_4 anions have been omitted for clarity.

Table 4.6: Crystal system and refinement data of complex **2**.

Complex	**2**
Empirical formula	$C_{40}H_{36}N_{24}Ni_4O_4Cl_4O_4$
Formula weight	1549.49
Crystal system	tetragonal
Space group	$I4_1/amd$
a/Å	13.787(5)
b/Å	13.787(5)
c/Å	40.518(5)
α/o	90
β/o	90
ɣ/o	90
Volume/Å3	7702(6)
Z	4
ρcalc g/cm3	1.336
μ/mm-1	1.173
F(000)	3136.0
Crystal size/mm3	0.366 × 0.307 × 0.282
Radiation	Mo Kα (λ = 0.71073)
θ range for data collection	4.1732 to 54.9672
Reflections collected	15060
Independent reflections	2398[R_{int}= 0.0228, R_{sigma}= N/A]
Data/restraints/parameters	2398/18/111
Goodness-of-fit on F2	1.051
Final R indices [I > 2σ(I)]	R_1 = 0.0732, wR_2 = 0.2152

Table 4.6,continued.

R indices (all data)	R_1 = 0.0812, wR_2 = 0.2226

Table 4.7: Selected bond lengths (Å) and bond angles (°) of complex **2**.

Bond lengths (Å)		**Bond angles (°)**	
Ni1-N1	2.078(4)	N3-Ni1-N3[3]	177.8(2)
Ni1-N3	2.040(4)	N3-Ni1-N1	76.99(16)
Ni1-O1	2.089(2)	N3[3]-Ni1-N1	101.37(16)
Ni1[2]-O1	2.089(2)	N3-Ni1-N1[3]	101.37(16)
Ni1-Ni1	3.475(0)	N3[3]-Ni1-N1[3]	76.99(16)
		N1-Ni1-N13	88.0(2)
		N3-Ni1-O1[3]	91.04(14)
		N3[3]-Ni1-O1[3]	90.64(13)
		N1-Ni1-O1[3]	167.91(15)
		N1[3]-Ni1-O1[3]	96.14(15)
		N3-Ni1-O1	90.64(13)
		N3[3]-Ni1-O1	91.04(14)
		N1-Ni1-O1	96.14(15)
		N1[3]-Ni1-O1	167.91(15)
		O1[3]-Ni1-O1	82.2(2)

[2]+X,1/2-Y,+Z; [3]3/4-Y,3/4-X,1/4-Z

Crystallisation of complex **3** by vapour diffusion technique from acetonitrile/diethyl ether solvent system formed dark red orange coloured crystal which was analysed by X-ray diffraction. X-ray crystal structure analysis revealed that the complex was centrosymmetric and adopted a slightly distorted octahedral geometry. Complex **3** was crystallised in orthorhombic Cmmm space group. The asymmetric unit and coordination environment of Co atom was shown in Figure 4.13 and Figure 4.14 respectively. Each Co

central atom is surrounded octahedrally by two neutral tetradentate ligands in a *cis*-isomer arrangement and bridged by one oxo ligand and one methoxy ligand. The bridging ligands formation occurred due to the utilisation of DBU as a base together with coordinating solvent, methanol during the complexation process. Each Co atom is coordinated with four nitrogen atoms (N1, N3, N4, N6) of two **L1** ligands and two oxygen atoms ((O1, O2) of oxo and methoxy bridging, respectively. The hydrogen atoms (H1, H1A, H2, H2A, H3, H3A) bonded to H-C1-O2 (methoxy group) exhibited a peculiar behaviour. It is a reasonable postulation that this freely rotating hydrogen atoms on $-CH_3$ with the occupancy of 0.5 exposed six hydrogen atoms instead of three hydrogen atoms due to the existence of 2-fold axis (Müller, 2009). Similarly, the bulkiness and symmetric characteristic by the ligand, the octahedral coordination spheres of the central Co atoms were slightly distorted. Two Co(II/III) centres were bridged by the ligand to form a twelve-membered macrocycle which adopts a boat configuration. In this type of ring, the four Co(II/III) centres were exactly coplanar to present a square configuration (Gao *et al.*, 2006). The crystal system and refinement data were shown in Table 4.8. Selected bond lengths were shown in Table 4.9.

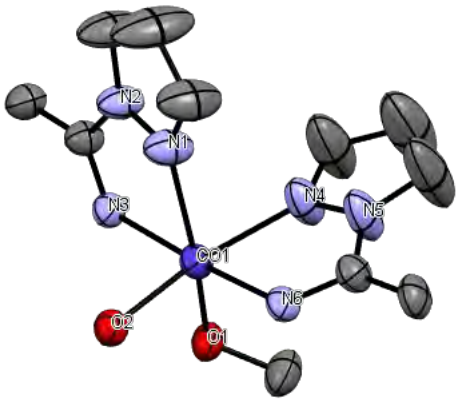

Figure 4.13: Asymmetric X-ray crystal structure of complex **3**, $[Co_4(C_{10}H_8N_6)_4(\mu\text{-}CH_3O)_2(\mu\text{-}O)_2](PF_6)_3(NO_3)$ with thermal ellipsoids (50% probability). Hydrogen atoms and the four PF_6 anions have been omitted for clarity.

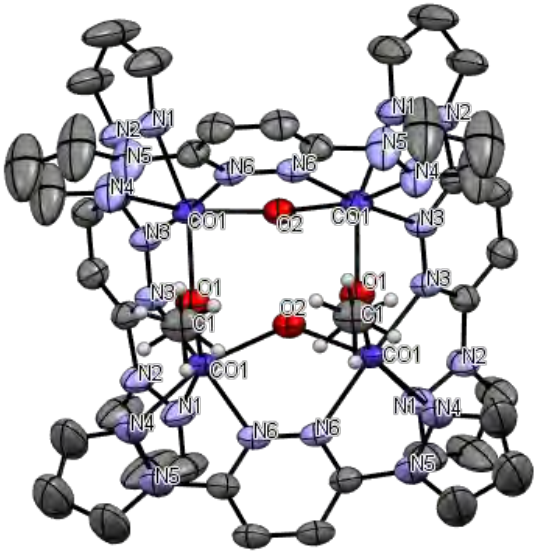

Figure 4.14: Overall X-ray crystal structure of complex **3**, $[Co_4(C_{10}H_8N_6)_4(\mu\text{-}CH_3O)_2(\mu\text{-}O)_2](PF_6)_3(NO_3)$ with thermal ellipsoids (50% probability). Hydrogen atoms and the four PF_6 anions have been omitted for clarity.

Table 4.8: Crystal system and refinement data of complex **3**.

Complex	**3**
Empirical formula	$C_{42}H_{38}Co_4F_{18}N_{26}O_{10}P_3$
Formula weight	1737.61
Crystal system	orthorhombic
Space group	Cmmm
a/Å	13.926(5)
b/Å	41.612(5)
c/Å	14.527(5)
α/o	90.000(5)
β/o	90.000(5)
ɣ/o	90.000(5)
Volume/Å3	8418(4)
Z	4

Table 4.8, continued.

ρcalc g/cm3	1.371
μ/mm-1	0.928
F(000)	3468.0
Crystal size/mm3	0.261 x 0.16 x 0.124
Radiation	MoKα (λ = 0.71073)
θ range for data collection	4.168 to 54.968
Reflections collected	22408
Independent reflections	5286 [R_{int} = 0.0319, R_{sigma} = 0.0343]
Data/restraints/parameters	5286/51/261
Goodness-of-fit on F2	1.110
Final R indices [I > 2σ(I)]	R1 =0.0662, wR2 = 0.2141
R indices (all data)	R1 = 0.0807, wR2 =0.2272

Table 4.9: Selected bond lengths (Å) and bond angles (°) of complex **3**.

Bond lengths (Å)		**Bond angles (°)**	
Co1-O2	2.0991 (19)	O2-Co1-N3	90.85(11)
Co1-O1	1.9794 (18)	O2-Co1-N6	88.98(11)
Co1-N3	2.105 (3)	O2-Co1-N1	97.32(14)
Co1-N6	2.131 (3)	O2-Co1-N4	162.67(13)
Co1-N1	2.178 (3)	O1-Co1-O2	92.55(13)
Co1-N4	2.161 (3)	O1-Co1-N3	86.36(12)
		O1-Co1-N6	99.21(12)
		O1-Co1-N1	157.78(13)
		O1-Co1-N4	94.06(15)

Table 4.9, continued.

		N3-Co1-N6	174.43(11)
		N3-Co1-N1	73.68(12)
		N3-Co1-N4	105.53(12)
		N6-Co1-N1	100.82(11)
		N6-Co1-N4	74.15(12)
		N4-Co1-N1	82.29(16)
		Co1[2]-O2-Co1	116.04(15)
		Co1-O1-Co1[5]	118.56(17)

[2]1-X,+Y,+Z; [5]+X,+Y,-Z

4.7 Electrochemical behaviour analyses

4.7.1 Cyclic voltammetry analyses

(a) Ligand, L1

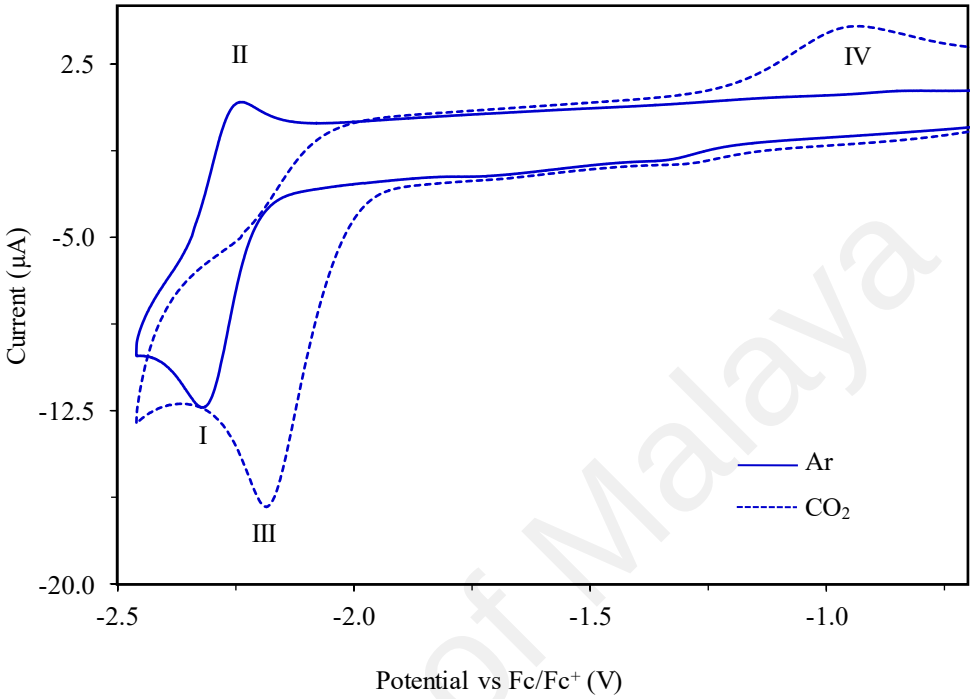

Figure 4.15: Cyclic voltammograms of 0.5 mM of **L1** with 0.1 M of TBAP in 2 mL of DMF under Ar and CO_2 at a scan rate of 100 mVs^{-1}.

The electrochemical properties of **L1** and complex **1-3** were investigated using cyclic voltammetry (CV) under inert (Ar for complex **1**, **2** & N_2 for complex **3**) and CO_2 saturated environments in DMF solution with 0.1 M TBAP as supporting electrolyte. Figure 4.15 illustrates the cyclic voltammograms of **L1** under Ar and CO_2. Under the Ar condition, one reversible redox couple with a formal potential of −2.30 V (peak I/II) was observed as indicated in Figure 4.15 (peak-to-peak separation = ~60 mV). With the reference previous studies, reduction of **L1 (L1$^{\bullet-}$)** is assigned to the peak I/II (Dai *et al.*, 2009; Steel, & Constable, 1990). The reversible redox couple corresponds to the reduction/oxidation process of the ligand that involves the transfer of one electron.

When the cell is purged with CO_2, the cathodic wave which observed earlier was positively shifted to −1.80 V with a loss in reversibility indicating an interaction between the reduced **L1 (L1$^{\bullet-}$)** and CO_2. This kind of interaction with CO_2 decreases the electronic density on the ligand thus making it more effortlessly to be reduced. The appearance of new oxidation peak IV at −0.94 V is presumably due to the product reduction at peak III.

(b) ***Metal complexes***

i Inert atmosphere

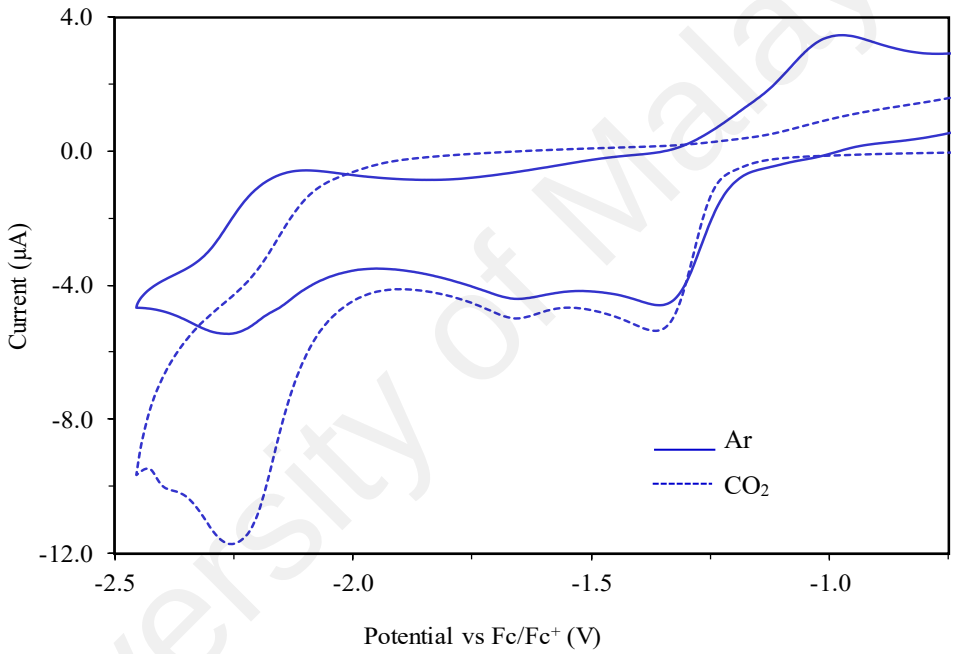

Figure 4.16: Cyclic voltammograms of 0.5 mM of complex **1** with 0.1 M of TBAP in 2 mL of DMF under Ar and CO_2 at a scan rate of 100 mVs^{-1}.

Complexes **1** - **3** displayed very distinct redox behaviours as indicated in Figure 4.16 - Figure 4.18. In general, these complexes exhibited both metal-localised and ligand-localised redox processes (Dai *et al.*, 2009). Dinuclear complex **1** demonstrates two reduction waves (Figure 4.16) which is consistent with the reduction of nickel centres from Ni^{II} to Ni^{I} at the potential −1.34 V and −1.66 V respectively. The quasi-reversible reduction peak attributed to the reduction of the ligand moieties were located at $E_{pc/pa}$ =

−2.27 V (~120 mV peak to peak separation). An irreversible oxidation peak appeared at −0.99 V when scanning towards the positive region. This proposes either sluggish kinetics in the oxidation of this complex or increased instability of the electrochemically reduced species (Simón Manso, & Kubiak, 2005).

Figure 4.17 shows the CV of tetranuclear complex **2** under Ar atmosphere. Reduction peak at E_{pc} = −1.46 V was assigned to Ni(II/I) redox couple while the ligand-based reduction was located at $E_{pc/pa}$ = −2.31 V (~123 mV peak to peak separation). The irreversible nature of electrochemical reductions could be explained due to the structural rearrangements which give rise to more stable reduced species (Simón Manso, & Kubiak, 2005).

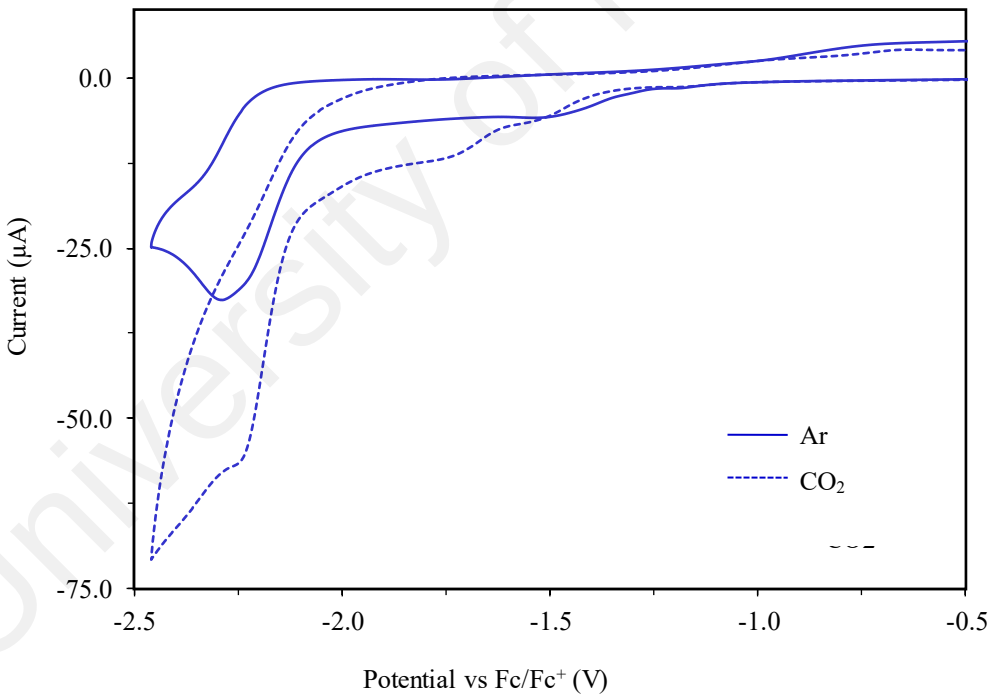

Figure 4.17: Cyclic voltammograms of 0.5 mM of complex **2** with 0.1 M of TBAP in 2 mL of DMF under Ar and CO_2 at a scan rate of 100 mVs^{-1}.

Tetranuclear complex **3** showed one reduction wave (Figure 4.18) at the potential of -1.24 V due to the reduction of cobalt centres from Co^{III} to Co^{II}. The quasi-reversible reduction peak attributed to the reduction of the ligand moieties were located at $E_{pc/pa}$ = -2.16 V (~ 180 mV peak to peak separation). On the other hand, Lam and co-workers assigned their complex $[Co(qtpy)(OH_2)_2]^{2+}$ reduction from Co^{III} to Co^{II} as quasi reversible. In their case, the quaterpyridine ligand shows an irreversible peak (Che *et al.*, 1988). Two irreversible oxidation peaks appeared at −0.69 V and -0.23 V when scanning towards a positive region. This displays a similar phenomenon as complex **1**.

ii CO_2 atmosphere

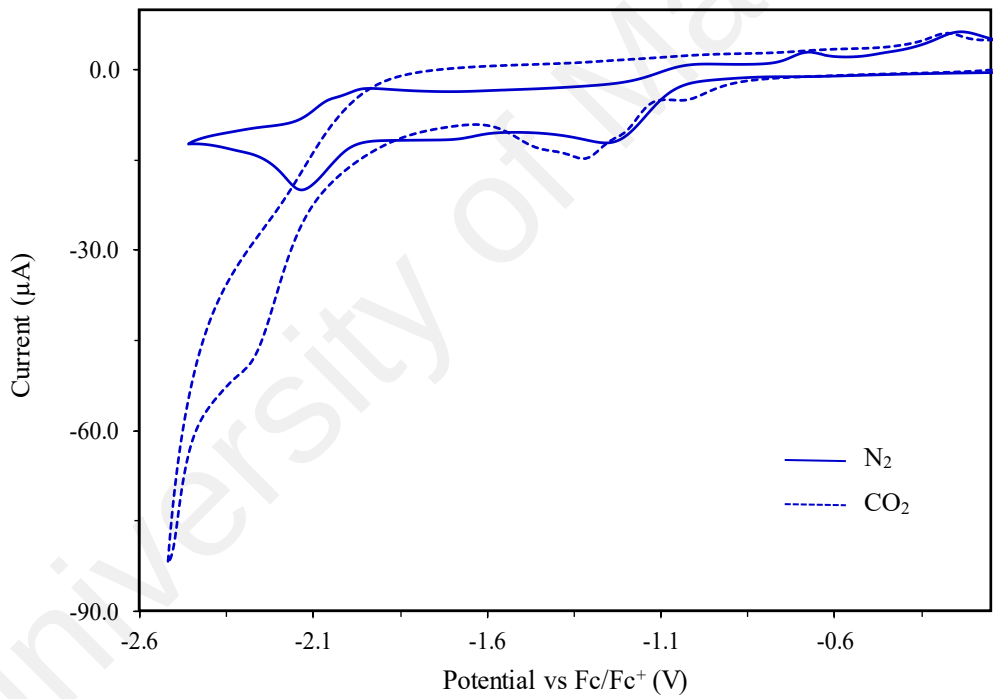

Figure 4.18: Cyclic voltammograms of 0.5 mM of complex **3** with 0.1 M of TBAP in 2 mL of CH_3CN under N_2 and CO_2 at a scan rate of 100 mVs^{-1}.

In the presence of CO_2, the CV of complex **1** showed a large current enhancement at −2.20 V (Figure 4.16). For complex **2**, a new reduction peak appeared at E_{pc} = −1.71 V followed by a current enhancement at −1.97 V (Figure 4.17). Similarly, complex **3** displayed a current enhancement at -1.89 V followed by shifting peak from -2.16 V to -

2.26 V as shown in Figure 4.18. In complexes **1** and **2**, the quasi-reversible reduction peaks at ~−2.25 V became irreversible and were positively shifted under CO_2 environment (~46 mV for complex **1** and ~148 mV for complex **2**).). The positive shift is suggested that the CO_2 binds to the reduced Ni(I) species (Froehlich, & Kubiak, 2015; Simón Manso, & Kubiak, 2005). For this case, in the absence of proton source, Kubiak and co-workers reported two possibilities for the irreversibility for their $[Ni(cyclam)]^{2+}$ complexes either CO_2 binding is an irreversible process or existence of fast, irreversible chemical step following CO_2 binding or ECC mechanism (Froehlich, & Kubiak, 2015; Kelly *et al.*, 1995; Simón Manso, & Kubiak, 2005). For complex **3** the quasi reversible peak at -2.16 V was developed into irreversible and it was negatively shifted under CO_2 environment as shown in Figure 4.18. Albeit, the uniqueness compared to complex **1** and **2**, this still disclosed the interaction of Co(II/I) species with carbon dioxide. Thus, controlled-potential electrolysis (CPE) experiments were carried out to clarify such incidents. Summary of electrochemical parameters under inert and CO_2 environment presented in Table 4.10 and Table 4.11 respectively.

Table 4.10: Electrochemical parameters of complexes **1 - 3** under Ar/N_2.

Complex	E_{pc1}	E_{pc2}	$E_{pc/pa}$[a]	E_{pa1}	E_{pa2}
1	-1.34 V	-1.66 V	-2.27 / -2.15 V	-0.99 V	-
2	-1.46 V	-	-2.31 / -2.19 V	-	-
3	-1.24 V	-	-2.16 / -1.98 V	-0.69 V	-0.23 V

[a] quasi-reversible. All potentials were referenced to Fc/Fc^+

Table 4.11: Electrochemical parameters of complexes **1 - 3** under CO_2.

Complex	E_{pc1}	E_{pc2}	E_{pc3}
1	-1.37 V	-1.67 V	-2.20 V
2	-1.50 V	-1.71 V	-1.97 V

Table 4.11,continued

3	-1.32 V	-2.26 V	-

All potentials were referenced to Fc/Fc^+

4.7.2 Controlled potential electrolysis (CPE)

CPE for complexes **1** and **2** was carried out at the potential of −2.3 V under CO_2 for 60 minutes. Refer to Figure 4.19 and Figure 4.20. 0.17 µmol (2.02% Faradaic efficiency) of CO was detected for complex **2** after passing 1.59 C, whereas a negligible amount of CO was detected for complex **1** after passing of 1.29 C. The Faradaic efficiency is marginal as compared to mononuclear complexes reported in Appendix A- 2. Nonetheless, the activity of complex **1** and **2** is better comparing to multinuclear nickel complexes reported by the Schneider group and Dalaet group (DeLaet *et al.*, 1987; Schneider *et al.*, 2012a).

These findings proposed that the tetranuclear structure may provide a greater environment and stability for CO_2 reduction reaction. As a shred of evidence, the distance between Ni-Ni of complex **2** (3.475(1) Å) is shorter as compared to complex **1** (3.885(0) Å) which indicates the bimetallic synergistic effect between Ni centres which enhances the selectivity for CO_2-to-CO conversion as proposed by Lu.T.B et.al. (Cao *et al.*, 2018). The current enhancement in CV was partly due to CO_2 interaction with the complex **2**. Another possible reason for the current enhancement may attribute to the hydrogenation of the aromatic N-heterocycles ligand under reductive condition (Olu *et al.*, 2018).

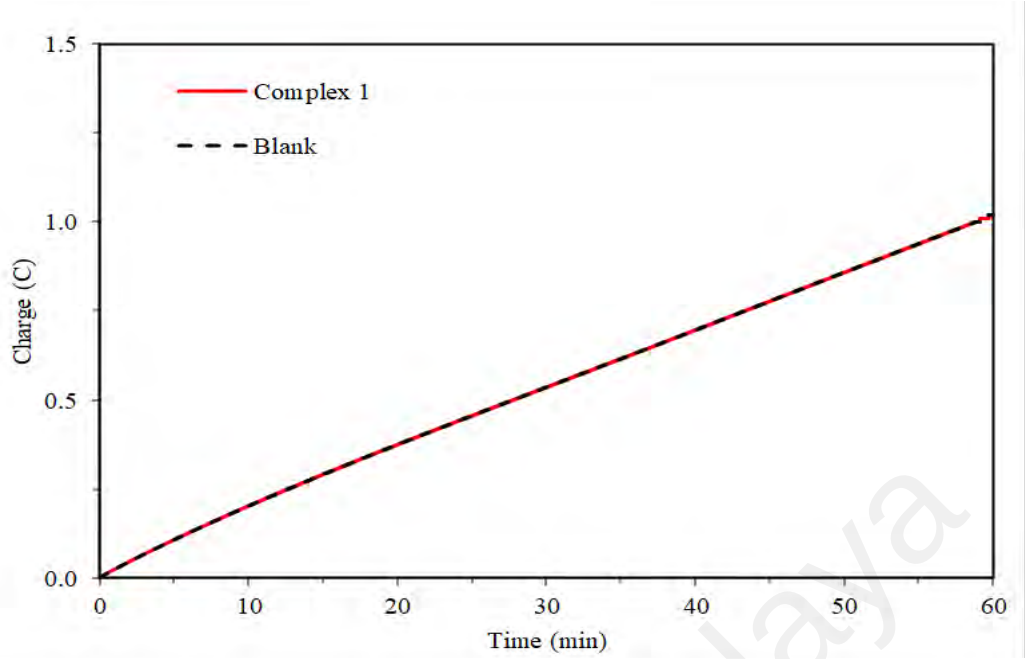

Figure 4.19: CPE was carried out in 2 compartmental cell with and without complex **1** under CO_2 in 0.1M TBAP/DMF on GC electrode for 1 h at -2.3 V.

Up to now, there is still a limited example of Ni complexes reported for electrochemical CO_2 reduction (Wang *et al.*, 2019), including mononuclear Ni polypyridyl derivatives (Elgrishi *et al.*, 2014; Lam *et al.*, 1995; Thoi *et al.*, 2013), mono- and dinuclear Ni cyclam derivatives (Cao *et al.*, 2018; Collin *et al.*, 1988), as well as di- and trinuclear Ni phosphine complexes (DeLaet *et al.*, 1987; Ratliff *et al.*, 1992). We demonstrate the potential use of multinuclear system linked with redox-active ligand was expected as the electron reservoir within the potential window that is suitable for CO_2 reduction. CPE for complex **3** was unable to complete due to limited resources and time.

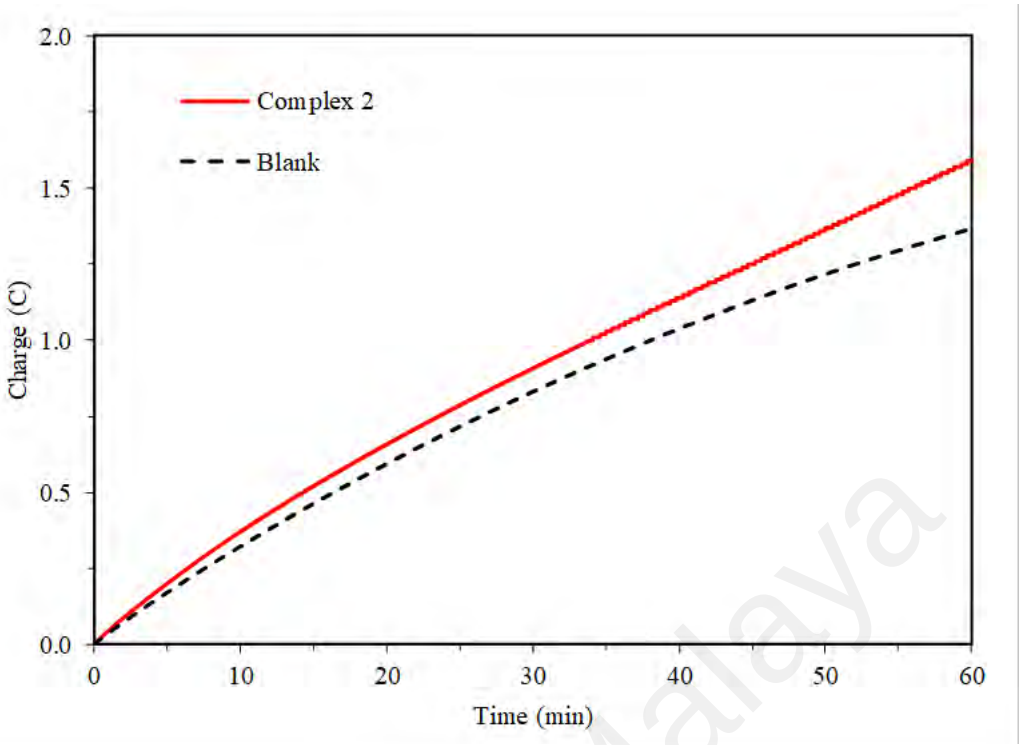

Figure 4.20: CPE was carried out in 2 compartmental cell with and without complex **2** under CO_2 in 0.1M TBAP/DMF on GC electrode for 1 hour at -2.3 V.

CHAPTER 5: CONCLUSION AND FURTHER STUDIES

5.1 Conclusion

This work summarises the construction of new multinuclear complexes and their characterisation. Dinuclear and tetranuclear Ni(II) complexes of bis(pyrazolyl)-pyridazine (**L1**) were selectively synthesised in the absence/presence of DBU as the base. The resulting complexes which showed the manner of complexes **1, 2,** and **3** were characterised by FTIR, single-crystal X-ray diffraction, and elemental analyses. In the presence of DBU, complexes **2** and **3** adapted the tetranuclear geometry coordination environment. However, complex **1** adapted dinuclear geometry coordination environment when DBU was not utilised in the synthesis. Therefore, a strong base such as DBU influences the complexation process.

The three complexes were tested for their behaviour as CO_2 reduction catalyst. Cyclic voltammetry study showed tetranuclear complexes **2** and **3** displayed stronger interaction with CO_2 as compared to complex **1**. The controlled-potential analysis which was conducted for complexes **1** and **2** revealed that the activity is marginal compared to other complexes reported towards CO_2 reduction. This scenario was assumed due to the greater environment and stability for CO_2 reduction reaction. Ni(II) and Co(III/II) complexes disclosed their molecular interface behaviour with CO_2 under electrochemical analysis.

5.2 Recommendation for further studies

The research has given a detailed insight into the structural properties of Ni(II) and Co(III/II) complexes. However, there is a lot of advancement that can be carried out in this research. For future work, controlled-potential electrolysis should be conducted for complex **3** to identify the form of carbon dioxide reduction products. Nevertheless, these multinuclear metal complexes were marginal active for CO_2 reduction under such conditions but may have possible applications for other catalytic redox reactions such as hydrogen evolution reaction and water oxidation reaction. Furthermore, the number of makeovers towards molecules structure can be designed such as choosing redox-active ligands and transition metals that active towards CO_2 reduction, designing unsaturated metal centre in a complex whereby the vacant site on the metal centre will able to coordinate small molecules with less hindrance.

REFERENCES

Alenezi, K. (2016). Electrocatalytic study of carbon dioxide reduction by Co(TPP)Cl complex. *Journal of Chemistry, 2016*, 1-7.

Altomare, A., Cascarano, G., Giacovazzo, C., Guagliardi, A., Burla, M. C., Polidori, G., & Camalli, M. (1994). SIR92-a program for automatic solution of crystal structures by direct methods. *Journal of Applied Crystallography, 27*(3), Article#435.

Anthony W. Addison, P. J. B. (1981). Synthesis of some imidazole- and pyrazole- derived chelating agents. *Journal of Heterocyclic Chemistry*(18), 803-805.

Appel, A. M., Bercaw, J. E., Bocarsly, A. B., Dobbek, H., DuBois, D. L., Dupuis, M., . . . Waldrop, G. L. (2013). Frontiers, opportunities, and challenges in biochemical and chemical catalysis of CO_2 fixation. *Chemical Reviews, 113*(8), 6621-6658.

Arana, C., Yan, S., Keshavarz K, M., Potts, K. T., & Abruna, H. D. (1992). Electrocatalytic reduction of carbon dioxide with iron, cobalt, and nickel complexes of terdentate ligands. *Inorganic Chemistry, 31*(17), 3680-3682.

Aresta, M., & Dibenedetto, A. (2007). Utilisation of CO_2 as a chemical feedstock: opportunities and challenges. *Dalton Transactions*(28), 2975-2992.

Aresta, M., Nobile, C. F., Albano, V. G., Forni, E., & Manassero, M. (1975). New nickel–carbon dioxide complex: synthesis, properties, and crystallographic characterization of (carbon dioxide)-bis(tricyclohexylphosphine)nickel. *Journal of the Chemical Society, Chemical Communications*(15), 636-637.

Ather, A. Q., Chaudhry, F., Khan, M. N., Silicz Bueno, E. A., Khan, M. A., Aslam, N., . . . Ejaz, S. A. (2013). Synthesis, antibacterial and antioxidant properties of pyrazolylpyridazines. *Asian Journal of Chemistry, 25*(14), 7743-7748.

Becker, K. D. (1992). N. W. Alcock: Bonding and structure, structural principles in inorganic and organic chemistry. *Berichte der Bunsengesellschaft für physikalische Chemie, 96*(1), 109-110.

Beley, M., Collin, J. P., Ruppert, R., & Sauvage, J. P. (1986). Electrocatalytic reduction of carbon dioxide by nickel cyclam^{2+} in water: study of the factors affecting the efficiency and the selectivity of the process. *Journal of the American Chemical Society, 108*(24), 7461-7467.

Benson, E. E., Kubiak, C. P., Sathrum, A. J., & Smieja, J. M. (2009). Electrocatalytic and homogeneous approaches to conversion of CO_2 to liquid fuels. *Chemical Society Reviews, 38*(1), 89-99.

Boot Handford, M. E., Abanades, J. C., Anthony, E. J., Blunt, M. J., Brandani, S., Mac Dowell, N., . . . Fennell, P. S. (2014). Carbon capture and storage update. *Energy & Environmental Science, 7*(1), 130-189.

Cao, L. M., Huang, H. H., Wang, J. W., Zhong, D. C., & Lu, T. B. (2018). The synergistic catalysis effect within a dinuclear nickel complex for efficient and selective electrocatalytic reduction of CO_2 to CO. *Green Chemistry, 20*(4), 798-803.

Chapovetsky, A., Do, T. H., Haiges, R., Takase, M. K., & Marinescu, S. C. (2016). Proton-assisted reduction of CO_2 by cobalt aminopyridine macrocycles. *Journal of the American Chemical Society, 138*(18), 5765-5768.

Che, C. M., Mak, S. T., Lee, W. O., Fung, K. W., & Mak, T. C. W. (1988). Electrochemical studies of nickel(II) and cobalt(II) complexes of tetra-azamacrocycles bearing a pyridine functional group and X-ray structures of $[Ni^{II}(L^3)Cl]ClO_4$ and $[Ni^{II}(L^3)][ClO_4]_2 \cdot H_2O$ {L^3=meso-2,3,7,11,12-pentamethyl-3,7,11,17-tetra-azabicyclo[11.3.1]heptadeca-1(17),13,15-triene}. *Journal of the Chemical Society, Dalton Transactions*(8), 2153-2159.

Chen, L., Guo, Z., Wei, X. G., Gallenkamp, C., Bonin, J., Anxolabéhère Mallart, E., . . . Robert, M. (2015). Molecular catalysis of the electrochemical and photochemical reduction of CO_2 with earth-abundant metal complexes. Selective production of CO vs HCOOH by switching of the metal center. *Journal of the American Chemical Society, 137*(34), 10918-10921.

Collin, J. P., Jouaiti, A., & Sauvage, J. P. (1988). Electrocatalytic properties of (tetraazacyclotetradecane)nickel(2+) and $Ni_2(biscyclam)^{4+}$ with respect to carbon dioxide and water reduction. *Inorganic Chemistry, 27*(11), 1986-1990.

Dai, F. R., Ye, H. Y., Li, B., Zhang, L. Y., & Chen, Z. N. (2009). Low-valence oxo-centred triruthenium complexes by bridging acetate substitution with pyrazolyldiazine or pyridinyltetrazine ligands. *Dalton Transactions*(40), 8696-8703.

DeLaet, D. L., Del Rosario, R., Fanwick, P. E., & Kubiak, C. P. (1987). Carbon dioxide chemistry and electrochemistry of a binuclear cradle complex of nickel(0), $Ni_2(\mu\text{-}CNMe)(CNMe)_2(PPh_2CH_2PPh_2)_2$. *Journal of the American Chemical Society, 109*(3), 754-758.

Do, J. Y., Chava, R. K., Mandari, K. K., Park, N.-K., Ryu, H.-J., Seo, M. W., . . . Kang, M. (2018). Selective methane production from visible-light-driven photocatalytic carbon dioxide reduction using the surface plasmon resonance effect of superfine silver nanoparticles anchored on lithium titanium dioxide nanocubes ($Ag@LixTiO_2$). *Applied Catalysis B: Environmental, 237*, 895-910.

Dobbek, Svetlitchnyi, H., Gremer, V., Huber, L., Meyer, R., & Ortwin. (2001). Crystal structure of a carbon monoxide dehydrogenase reveals a [Ni-4Fe-5S] cluster. *Science, 293*(5533), 1281-1285.

Dolomanov, O. V., Bourhis, L. J., Gildea, R. J., Howard, J. A. K., & Puschmann, H. (2009). OLEX2: a complete structure solution, refinement and analysis program. *Journal of Applied Crystallography, 42*(2), 339-341.

Dresselhaus, M. S., & Thomas, I. L. (2001). Alternative energy technologies. *Nature, 414*, 332-337.

Elgrishi, N., Chambers, M. B., Artero, V., & Fontecave, M. (2014). Terpyridine complexes of first row transition metals and electrochemical reduction of CO_2 to CO. *Physical Chemistry Chemical Physics, 16*(27), 13635-13644.

Fisher, B. J., & Eisenberg, R. (1980). Electrocatalytic reduction of carbon dioxide by using macrocycles of nickel and cobalt. *Journal of the American Chemical Society, 102*(24), 7361-7363.

Fogeron, T., Todorova, T. K., Porcher, J.-P., Gomez-Mingot, M., Chamoreau, L. M., Mellot-Draznieks, C., . . . Fontecave, M. (2018). A bioinspired nickel(bis-dithiolene) complex as a homogeneous catalyst for carbon dioxide electroreduction. *ACS Catalysis, 8*(3), 2030-2038.

Francke, R., & Little, R. D. (2014). Redox catalysis in organic electrosynthesis: basic principles and recent developments. *Chemical Society Reviews, 43*(8), 2492-2521.

Francke, R., Schille, B., & Roemelt, M. (2018). Homogeneously catalyzed electroreduction of carbon dioxide—methods, mechanisms, and catalysts. *Chemical Reviews, 118*(9), 4631-4701.

Froehlich, J. D., & Kubiak, C. P. (2012). Homogeneous CO_2 reduction by Ni(cyclam) at a glassy carbon electrode. *Inorganic Chemistry, 51*(7), 3932-3934.

Froehlich, J. D., & Kubiak, C. P. (2015). The homogeneous reduction of CO_2 by $[Ni(cyclam)]^+$: Increased catalytic rates with the addition of a CO scavenger. *Journal of the American Chemical Society, 137*(10), 3565-3573.

Gao, H., Zhang, Z. H., Jiang, P., & Li, X. R. (2006). Synthesis, crystal structures and properties of the novel mononuclear copper(II) and tetranuclear cobalt(II) complexes with 3,6-bis-(3,5-dimethylpyrazolyl)-pyridazine. *Transition Metal Chemistry, 31*(8), 1088-1092.

García Antón, J., Bofill, R., Escriche, L., Llobet, A., & Sala, X. (2012). Transition-metal complexes containing the dinucleating tetra-N-dentate 3,5-bis(2-pyridyl)pyrazole (Hbpp) ligand – a robust scaffold for multiple applications including the catalytic oxidation of water to molecular oxygen. *European Journal of Inorganic Chemistry, 2012*(30), 4775-4789.

Ghosh, S., & Baik, M.-H. (2011). The mechanism of O=O bond formation in tanaka's water oxidation catalyst. *Angewandte Chemie International Edition, 51*(5), 1221-1224.

Gupta, G., Prasad, K. T., Das, B., Yap, G. P. A., & Rao, K. M. (2009). Ruthenium half-sandwich complexes with tautomerized pyrazolyl-pyridazine ligands: Synthesis, spectroscopic and molecular structural studies. *Journal of Organometallic Chemistry, 694*(16), 2618-2627.

Gupta, G., Prasad, K. T., Rao, A. V., Geib, S. J., Das, B., & Rao, K. M. (2010). Novel mononuclear η^5-pentamethylcyclopentadienyl complexes of platinum group metals bearing pyrazolylpyridazine ligands: Syntheses and spectral studies. *Inorganica Chimica Acta, 363*(10), 2287-2295.

Jeoung, J. H., & Dobbek, H. (2007). Carbon dioxide activation at the Ni,Fe-cluster of anaerobic carbon monoxide dehydrogenase. *Science, 318*(5855), 1461-1464.

Johnson, T. C., Morris, D. J., & Wills, M. (2010). Hydrogen generation from formic acid and alcohols using homogeneous catalysts. *Chemical Society Reviews, 39*(1), 81-88.

Keene, F. R. (1993). Thermodynamic, kinetic, and product considerations in carbon dioxide reactivity. In K. K. B.R Sullivan, H.E. Guard (Ed.), *Electrochemical and electrocatalytic reactions of carbon dioxide* (pp. 1-16). Netherland: Elsevier Science Publishers B.V.

Kelly, C. A., Mulazzani, Q. G., Venturi, M., Blinn, E. L., & Rodgers, M. A. J. (1995). The Thermodynamics and Kinetics of CO_2 and H^+ Binding to Ni(cyclam)$^+$ in Aqueous Solution. *Journal of the American Chemical Society, 117*(17), 4911-4919.

Kleij, A. W. (2013). Carbon dioxide activation and conversion. In S. L. Suib (Ed.), *New and Future Developments in Catalysis* (pp. 559-587). Amsterdam: Elsevier.

Lam, K. M., Wong, K. Y., Yang, S. M., & Che, C. M. (1995). Cobalt and nickel complexes of 2,2′ : 6′ ,2″ : 6″ ,2‴-quaterpyridine as catalysts for electrochemical reduction of carbon dioxide. *Journal of the Chemical Society, Dalton Transactions*(7), 1103-1107.

Leitner, W. (1996). The coordination chemistry of carbon dioxide and its relevance for catalysis: a critical survey. *Coordination Chemistry Reviews, 153*, 257-284.

Li, Y., Liu, Q., Huang, W., & Yang, J. (2018). Solubilities of CO_2 capture absorbents methyl benzoate, ethyl hexanoate and methyl heptanoate. *The Journal of Chemical Thermodynamics, 127*, 25-32.

Liu, F. W., Bi, J., Sun, Y., Luo, S., & Kang, P. (2018). Cobalt complex with redox-active imino bipyridyl ligand for electrocatalytic reduction of carbon dioxide to formate. *ChemSusChem, 11*(10), 1656-1663.

Meshitsuka, S., Ichikawa, M., & Tamaru, K. (1974). Electrocatalysis by metal phthalocyanines in the reduction of carbon dioxide. *Journal of the Chemical Society, Chemical Communications*(5), 158-159.

Morris, A. J., Meyer, G. J., & Fujita, E. (2009). Molecular approaches to the photocatalytic reduction of carbon dioxide for solar fuels. *Accounts of Chemical Research, 42*(12), 1983-1994.

Müller, P. (2009). Practical suggestions for better crystal structures AU. *Crystallography Reviews, 15*(1), 57-83.

Nakamoto, K. (1988). Infrared and raman spectra of inorganic and coordination compounds. *Berichte der Bunsengesellschaft für physikalische Chemie, 92*(4), Article#561.

North, M., & Pasquale, R. (2009). Mechanism of cyclic carbonate synthesis from epoxides and CO_2. *Angewandte Chemie International Edition, 48*(16), 2946-2948.

Okamura, M., Kondo, M., Kuga, R., Kurashige, Y., Yanai, T., Hayami, S., . . . Masaoka, S. (2016). A pentanuclear iron catalyst designed for water oxidation. *Nature, 530*, 465-468.

Olu, P. Y., Li, Q., & Krischer, K. (2018). The true fate of pyridinium in the reportedly pyridinium-catalyzed carbon dioxide electroreduction on platinum. *Angewandte Chemie International Edition, 57*(45), 14769-14772.

Paparo, A., & Okuda, J. (2017). Carbon dioxide complexes: Bonding modes and synthetic methods. *Coordination Chemistry Reviews, 334*, 136-149.

Praneeth, V. K. K., Kondo, M., Okamura, M., Akai, T., Izu, H., & Masaoka, S. (2019). Pentanuclear iron catalysts for water oxidation: substituents provide two routes to control onset potentials. *Chemical Science, 10*(17), 4628-4639.

Praneeth, V. K. K., Ringenberg, M. R., & Ward, T. R. (2012). Redox-active ligands in catalysis. *Angewandte Chemie International Edition, 51*(41), 10228-10234.

Rakowski Dubois, M., & Dubois, D. L. (2009). Development of molecular electrocatalysts for CO_2 reduction and H_2 production/oxidation. *Accounts of Chemical Research, 42*(12), 1974-1982.

Ratliff, K. S., Lentz, R. E., & Kubiak, C. P. (1992). Carbon dioxide chemistry of the trinuclear complex $[Ni_3(\mu_3\text{-CNMe})(\mu_3\text{-I})(dppm)_3][PF_6]$. Electrocatalytic reduction of carbon dioxide. *Organometallics, 11*(6), 1986-1988.

Read, R. J., & Kleywegt, G. J. (2009). Low-resolution structure determination and validation. *Acta Crystallographica Section D, 65*(2), Article#1.

Rosas Hernandez, A., Steinlechner, C., Junge, H., & Beller, M. (2017). Photo- and electrochemical valorization of carbon dioxide using earth-abundant molecular catalysts. *Topics in Current Chemistry (Cham), 376*(1), Article#1.

Rountree, E. S., McCarthy, B. D., Eisenhart, T. T., & Dempsey, J. L. (2014). Evaluation of homogeneous electrocatalysts by cyclic voltammetry. *Inorganic Chemistry, 53*(19), 9983-10002.

Roy, S., Sharma, B., Pécaut, J., Simon, P., Fontecave, M., Tran, P. D., . . . Artero, V. (2017). Molecular cobalt complexes with pendant amines for selective electrocatalytic reduction of carbon dioxide to formic acid. *Journal of the American Chemical Society, 139*(10), 3685-3696.

Rudolph, M., Dautz, S., & Jäger, E. G. (2000). Macrocyclic $[N_4^{2-}]$ coordinated nickel nomplexes as catalysts for the formation of oxalate by electrochemical reduction of carbon dioxide. *Journal of the American Chemical Society, 122*(44), 10821-10830.

Sakakura, T., Choi, J. C., & Yasuda, H. (2007). Transformation of carbon dioxide. *Chemical Reviews, 107*(6), 2365-2387.

Sampson, M. D., Nguyen, A. D., Grice, K. A., Moore, C. E., Rheingold, A. L., & Kubiak, C. P. (2014). Manganese catalysts with bulky bipyridine ligands for the electrocatalytic reduction of carbon dioxide: eliminating dimerization and altering catalysis. *Journal of the American Chemical Society, 136*(14), 5460-5471.

Sangilipandi, S., Nagarajaprakash, R., Sutradhar, D., Kaminsky, W., Chandra, A. K., & Mohan Rao, K. (2015). Synthesis, molecular structural studies and DFT calculations of tricarbonylrhenium(I) metal complexes containing nitrogen based N∩N donor polypyridyl ligands. *Inorganica Chimica Acta, 437*, 177-187.

Savéant, J. M. (2008). Molecular catalysis of electrochemical reactions. Mechanistic aspects. *Chemical Reviews, 108*(7), 2348-2378.

Schneider, J., Jia, H., Kobiro, K., Cabelli, D. E., Muckerman, J. T., & Fujita, E. (2012a). Nickel(ii) macrocycles: highly efficient electrocatalysts for the selective reduction of CO_2 to CO. *Energy & Environmental Science, 5*(11), 9502-9510.

Schneider, J., Jia, H., Muckerman, J. T., & Fujita, E. (2012b). Thermodynamics and kinetics of CO_2, CO, and H^+ binding to the metal centre of CO_2 reduction catalysts. *Chemical Society Reviews, 41*(6), 2036-2051.

Schwarz, H. A., & Dodson, R. W. (1989). Reduction potentials of CO_2^- and the alcohol radicals. *The Journal of Physical Chemistry, 93*(1), 409-414.

Sheldrick, G. (2015a). Crystal structure refinement with SHELXL. *Acta Crystallographica Section C, 71*(1), 3-8.

Sheldrick, G. (2015b). SHELXT-Integrated space-group and crystal-structure determination. *Acta Crystallographica Section A, 71*(1), 3-8.

Simmons, J. M., Wu, H., Zhou, W., & Yildirim, T. (2011). Carbon capture in metal–organic frameworks—a comparative study. *Energy & Environmental Science, 4*(6), 2177-2185.

Simón Manso, E., & Kubiak, C. P. (2005). Dinuclear nickel complexes as catalysts for electrochemical reduction of carbon dioxide. *Organometallics, 24*(1), 96-102.

Steel, P. J., & Constable, E. C. (1990). Synthesis, spectroscopy, and electrochemistry of homo- and hetero-leptic ruthenium(II) complexes of new pyrazole-containing bidentate ligands. *Journal of the Chemical Society, Dalton Transactions*(4), 1389-1396.

Steiner, G., Gries, J., & Lenke, D. (1981). Syntheis and antihypertensive activity of new 6-heteroaryl-3-hydrazinopyridazine derivatives. *Journal of Medicinal Chemistry, 24*(1), 59-63.

Takeda, H., Cometto, C., Ishitani, O., & Robert, M. (2016). Electrons, photons, protons and earth-abundant metal complexes for molecular catalysis of CO_2 reduction. *ACS Catalysis, 7*(1), 70-88.

Thoi, V. S., Kornienko, N., Margarit, C. G., Yang, P., & Chang, C. J. (2013). Visible-light photoredox catalysis: Selective reduction of carbon dioxide to carbon monoxide by a Nickel N-heterocyclic carbene–isoquinoline complex. *Journal of the American Chemical Society, 135*(38), 14413-14424.

Tinnemans, A. H. A., Koster, T. P. M., Thewissen, D. H. M. W., & Mackor, A. (1984). Tetraaza-macrocyclic cobalt(II) and nickel(II) complexes as electron-transfer agents in the photo(electro)chemical and electrochemical reduction of carbon dioxide. *Recueil des Travaux Chimiques des Pays-Bas, 103*(10), 288-295.

Vidal Vázquez, F., Kihlman, J., Mylvaganam, A., Simell, P., Koskinen Soivi, M. L., & Alopaeus, V. (2018). Modeling of nickel-based hydrotalcite catalyst coated on heat exchanger reactors for CO_2 methanation. *Chemical Engineering Journal, 349*, 694-707.

Viswanathan, B. (2013). Electro-catalytic reduction of carbon dioxide. In S. L. Suib (Ed.), *New and Future Developments in Catalysis* (pp. 275-295). Amsterdam: Elsevier.

Vol'pin, M. E., & Kolomnikov, I. S. (1973). Reactions of CO_2 with transition metal compounds. *Pure and Applied Chemistry, 33*(4), 567-582.

Volbeda, A., & Fontecilla Camps, J. C. (2005). Structural bases for the catalytic mechanism of Ni-containing carbon monoxide dehydrogenases. *Dalton Transactions*(21), 3443-3450.

Wada, T., Tsuge, K., & Tanaka, K. (2000). Electrochemical oxidation of water to dioxygen catalyzed by the oxidized form of the bis(ruthenium – hydroxo) complex in H_2O. *Angewandte Chemie International Edition, 39*(8), 1479-1482.

Wada, T., Tsuge, K., & Tanaka, K. (2001). Syntheses and redox properties of bis(hydroxoruthenium) complexes with quinone and bipyridine ligands. Water-oxidation catalysis. *Inorganic Chemistry, 40*(2), 329-337.

Wang, J. W., Liu, W. J., Zhong, D. C., & Lu, T. B. (2019). Nickel complexes as molecular catalysts for water splitting and CO_2 reduction. *Coordination Chemistry Reviews, 378*, 237-261.

Wang, W. H., Himeda, Y., Muckerman, J. T., Manbeck, G. F., & Fujita, E. (2015). CO_2 hydrogenation to formate and methanol as an alternative to photo- and electrochemical CO_2 reduction. *Chemical Reviews, 115*(23), 12936-12973.

Wu, Y., Rudshteyn, B., Zhanaidarova, A., Froehlich, J. D., Ding, W., Kubiak, C. P., & Batista, V. S. (2017). Electrode-ligand interactions dramatically enhance CO_2 conversion to CO by the $[Ni(cyclam)](PF_6)_2$ catalyst. *ACS Catalysis, 7*(8), 5282-5288.

Yamase, T., & Sugeta, M. (1990). Photoreduction of CO_2 to CH_4 in water using dititanodecatungstophosphate as multielectron transfer catalyst. *Inorganica Chimica Acta, 172*(2), 131-134.

Zhang, M., El Roz, M., Frei, H., Mendoza Cortes, J. L., Head Gordon, M., Lacy, D. C., & Peters, J. C. (2015). Visible light sensitized CO_2 activation by the tetraaza

$[Co^{II}N_4H(MeCN)]^{2+}$ complex investigated by FT-IR spectroscopy and DFT calculations. *The Journal of Physical Chemistry C, 119*(9), 4645-4654.

Zhang, Q., & Guan, J. (2019). Mono-/multinuclear water oxidation catalysts. *ChemSusChem, 12*(14), 3209-3235.

Zhu, X. J., & Holliday, B. J. (2010). Electropolymerization of a ruthenium(II) bis(pyrazolyl)pyridine complex to form a novel Ru-containing conducting metallopolymer. *Macromolecular Rapid Communications, 31*(9 - 10), 904-909.